NASA TECHNICAL NOTE

NASA TN D-5064

C.1

NASA TN D-5064

TWO DIMENSIONAL INVISCID JET FLOW FROM TWO NOZZLES AT AN ANGLE TO A PLANE SURFACE

by Marvin E. Goldstein and Robert Siegel

Lewis Research Center
Cleveland, Ohio

NATIONAL AERONAUTICS AND SPACE ADMINISTRATION • WASHINGTON, D. C. • FEBRUARY 1969

NASA TN D-5064

TWO DIMENSIONAL INVISCID JET FLOW FROM TWO NOZZLES AT AN ANGLE TO A PLANE SURFACE

By Marvin E. Goldstein and Robert Siegel

Lewis Research Center
Cleveland, Ohio

NATIONAL AERONAUTICS AND SPACE ADMINISTRATION

For sale by the Clearinghouse for Federal Scientific and Technical Information
Springfield, Virginia 22151 – CFSTI price $3.00

ABSTRACT

Conformal mapping was used to obtain the free streamlines and wall pressure coefficient for jets issuing from two nozzles and striking a surface. The jet nozzle exit planes are at an angle to the surface and can be spaced an arbitrary distance apart and an arbitrary distance from the surface. The effect of nozzle position and tilt anlge on the extent of the flow back between the nozzles is shown. The back flow results from a collision between part of the flow from each jet that has been turned by striking the plate.

TWO DIMENSIONAL INVISCID JET FLOW FROM TWO NOZZLES AT AN ANGLE TO A PLANE SURFACE

by Marvin E. Goldstein and Robert Siegel

Lewis Research Center

SUMMARY

Conformal mapping was used to obtain the free streamlines and wall pressure coefficient for jets issuing from two nozzles and striking a surface. The jet nozzle exit planes are at an angle to the surface and can be spaced an arbitrary distance apart and an arbitrary distance from the surface. The effect of nozzle position and tilt angle on the extent of the flow back between the nozzles is shown. The back flow results from a collision between part of the flow from each jet that has been turned by striking the plate.

INTRODUCTION

Single and multiple fluid jets of various cross-sections and in various orientations impinging on surfaces are used in a number of fluid mechanical devices and industrial heat and mass transfer applications. These include ground effect machines, V/STOL aircraft, cooling of steel strip, tempering of glass and drying of paper. Some of the heat transfer applications are discussed in reference 1.

The impingement features of jets are not fully known, especially in the case of multiple jets. Some insight can be obtained by considering inviscid slot jets, as these can usually be analyzed by employing conformal transformations. An example is reference 2 where the flow pattern was determined for two parallel jets striking a plate. The potential flow solution is required to compute the boundary layer along the surface needed to determine the heat transfer or mass transfer.

This report presents an analytical solution for the flow field produced by two inviscid two-dimensional jets striking a plane surface. The jet nozzle openings are at an angle to the surface as shown in sketch (a), and the surrounding fluid is stationary. The study was undertaken to provide a qualitative picture of the flow pattern under a vertical take-off aircraft with a fan pod in each wing as shown in plan view in sketch (b). Although the computed flow is idealized, it is hoped that it will lead to an increased understanding of

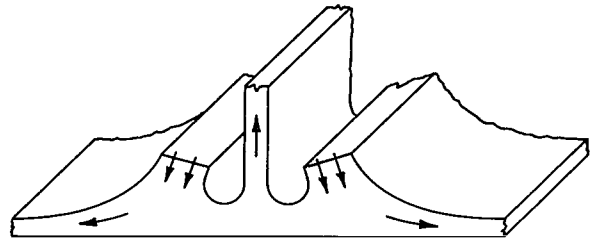

(a) Impingement of flow from two nozzles at an angle to a surface.

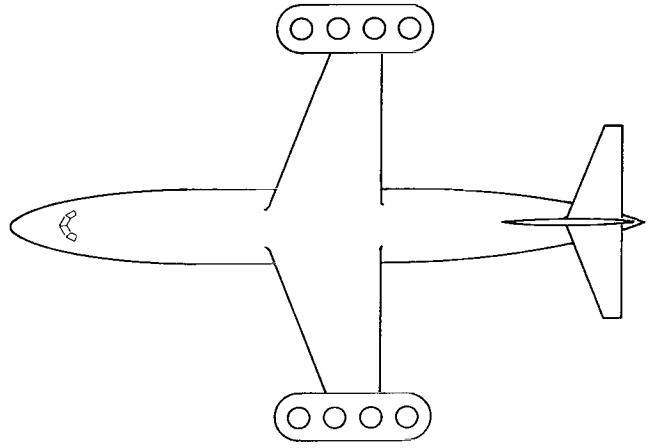

(b) Fan-pod configuration for VTOL aircraft.

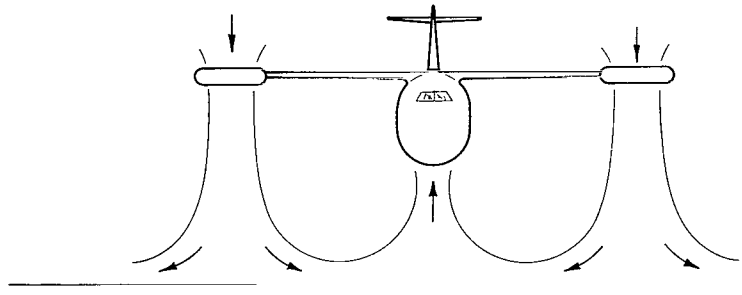

(c) Flow pattern from impinging jets under VTOL aircraft.

some aspects of the flow field beneath the aircraft. A consideration in the aircraft design is the recirculation upward under the fuselage as illustrated in sketch (c). Although this can provide a beneficial lifting force it can also provide an undesirable circulation around poritions of the aircraft of hot gases carrying debris from the ground (refs. 3 to 5). If the engines are tilted outward, the recirculation may be reduced, and for a sufficiently large tilting there will be no recirculation. In a real jet there is entrainment along the free streamlines and this will attenuate the velocities of the jet as it moves through the surrounding fluid. However, if the jet is only a few nozzle widths from the ground, the entrainment will be small and an inviscid solution will provide a reasonable guide to the flow distribution.

Within the assumptions of inviscid slot jets in constant pressure stationary surroundings, the flow patterns obtained here are exact solutions. The basic theory of conformal mapping as applied to jets is given in reference 6 among others. The flow configuration in the physical plane is found by carrying out an integration of the velocity potential multiplied by the reciprocal of the complex conjugate velocity. Conformal mapping is used to find the functional relation between the potential and velocity so that the integration can be performed.

The flow pattern will depend on the boundary condition at the nozzle. It is assumed here that the flow exits normal to the nozzle opening, which is a reasonable assumption for small nozzles or when turning vanes are used. This provides a nonuniform velocity distribution leaving the nozzle as a result of the flow interaction with the ground; the velocity in the central part of the nozzle is reduced relative to that along the sides of the nozzle. Numerical results will be given for the velocity profile at the nozzle exit, the free streamlines bounding the flow and the pressure coefficient along the ground.

SYMBOLS

A	a constant
A_0	a constant
C_0	a constant
C_P	pressure coefficient
I	flow region in the ξ plane
J	flow region in the W plane
K	complete elliptic integral of the first kind
K'	defined by $K'(k) = K(k')$
k	modulus of elliptic integral

k'	defined as $\sqrt{1 - k^2}$
p	pressure
p_o	ambient pressure outside jets
Q	functions defined in eqs. (B-4) and (B-5)
R	functions defined in eqs. (B-2) and (B-3)
T	complex variable in T-plane, $\xi + i\eta$
t	complex variable in t-plane
u	velocity in x direction
V	velocity
V_I	velocity at nozzle exit
$\overline{V}_I$	average velocity at nozzle exit
V_o	velocity along free streamlines
v	velocity in y direction
W	complex potential, $\varphi + i\psi$
X_N, Y_N	coordinates of center of nozzle exit plane nondimensionalized by Δ
x, y	coordinates in physical plane
z	complex variable, $x + iy$
α	tilt angle of nozzle, sketch (d)
Γ	flow region in the T-plane
Δ	width of nozzle
δ_L, δ_R	asymptotic widths of streams flowing to left and to right
ζ	complex conjugate velocity, $u - iv$
ϑ	Theta-function
ξ, η	coordinates of T-plane
ρ	density
τ^+	quantity defined as $iK'/2K$
φ	velocity potential
ψ	stream function
Ω	function defined in eq. (3)

Subscripts:

G, H refer to stagnation points, sketch (d)

r refers to boundary point, sketch(i)

Superscripts:

* complex conjugate

+ variables defined in eq. (B-1)

ANALYSIS

The flow configuration as shown in sketch (a) is symmetric about a vertical plane centered between the nozzles, hence only half the flow field need be considered. The boundaries in the physical plane (z plane) are shown in sketch (d). Since the region outside the jets is at constant pressure, the Bernoulli equation shows that the velocity has a constant magnitude along the free streamlines $\widehat{DE}$ and $\widehat{CF}$. The direction of the velocity on $\widehat{GF}$ and $\widehat{GHE}$ must be along the boundaries, which correspond respectively to the plane of symmetry and the ground. The point H is a stagnation point at which the direction of the velocity along $\widehat{GHE}$ must reverse. The dashed line is a streamline dividing the portions of the flow that go to the right along the ground or to the left into the stream that flows back upward. The point G is a stagnation point. Along the nozzle exit $\widehat{CD}$ the velocity is specified as being perpendicular to the line $\widehat{CD}$ and hence is of constant direction.

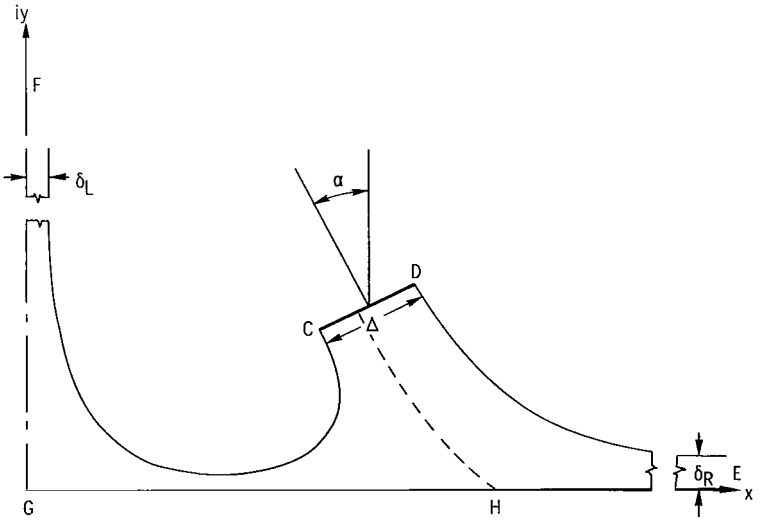

(d) Boundaries in physical plane (z-plane) where z = x + iy.

Let ζ be the complex conjugate velocity u - iv. From the velocity conditions on the flow boundaries it is deduced that the flow field in sketch (d) maps into the interior of the region I shown in sketch (e) of the hodograph plane (ζ-plane). (Corresponding points in the various planes are denoted by the same letters). The free streamlines map into portions of a circle since they have a constant velocity magnitude. The velocity at the nozzle exit maps into a cut at constant angle.

Let $W = \varphi + i\psi$ be the complex potential of the flow, where φ is the velocity potential and ψ is the stream function. The following considerations show that the flow field maps into the interior of the region J in sketch (f). Since the velocities are perpendicular to the nozzle exit, the streamlines (lines of constant ψ) must intersect the nozzle

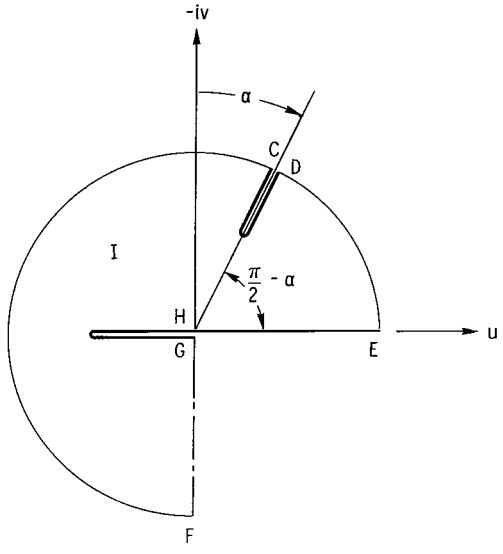

(e) Hodograph plane (ζ-plane) where $\zeta = u - iv$.

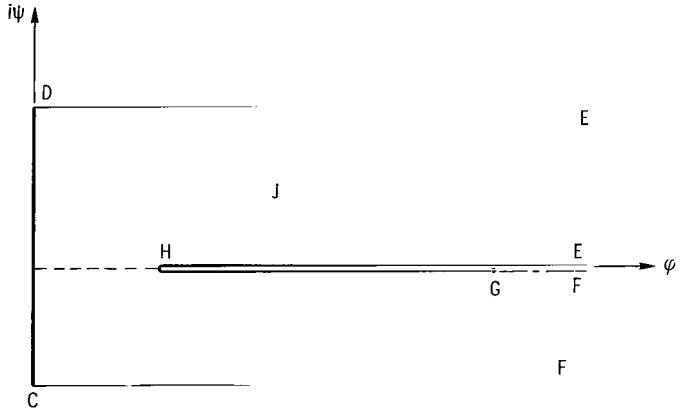

(f) Complex potential plane (W-plane) where $W = \varphi + i\psi$.

exit $\widehat{CD}$ at right angles. Then since the equal potential lines also intersect the streamlines at right angles, we conclude that the nozzle exit $\widehat{CD}$ must be a line of constant φ. The stream function ψ is constant along the free streamlines $\widehat{DE}$ and $\widehat{CF}$ and along the boundary streamlines $\widehat{FGHE}$. The dividing streamline of the flow must extend from a point on the nozzle exit to the stagnation point H. It follows from these conditions that the flow being considered maps into the interior of the region J shown in sketch (f) of the complex potential plane (W-plane).

In order to obtain the solution of the problem the known flow configuration in the potential plane is mapped into the physical plane by performing the integration

$$z = \int \frac{1}{\zeta} dW + \text{constant} \tag{1}$$

To carry out this integration the functional relation must be known between ζ and W.

To find the relation between ζ and W it is sufficient (ref. 6) to map some region Γ of an intermediate T-plane ($T = \xi + i\eta$) conformally onto[1] the region I of the hodograph plane and also conformally onto the region J of the W-plane. If ζ and W are the functions that will respectively map Γ onto I and J, it is necessary that ζ and W map the boundary of Γ onto the boundaries of I and J respectively. If γ is any section of the boundary of Γ such that $\zeta(\gamma)$ is one of the labeled sections of the boundary of I shown in sketch (e), $W(\gamma)$ must be the corresponding section of the boundary of J shown in sketch (f).

A convenient region to work with in the T-plane is a rectangle. As will be shown the region I in sketch (e) can be mapped into a rectangle by use of Theta-functions. The region J in sketch (f) is a generalized polygon which can be mapped into the upper half of the t-plane in sketch (g) by a Schwarz-Christoffel transformation. Then a second applica-

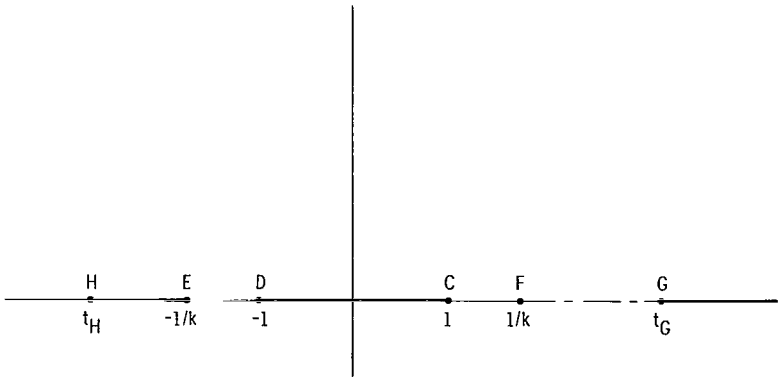

(g) Intermediate t-plane.

[1]The term "onto" includes the region and its boundary.

tion of the Schwarz-Christoffel transformation will relate the rectangle in the T-plane to the upper half of the t-plane. These transformations will involve elliptic functions.

Let $K = K(k)$ be the complete elliptic integral of the first kind of modulus k, $0 < k < 1$. Thus (ref. 7)

$$K = \int_0^{\pi/2} \frac{d\omega}{\sqrt{1 - k^2 \sin^2 \omega}} \tag{2}$$

and let $K' = K'(k)$ be defined by

$$K'(k) = K(k')$$

where

$$k' = \sqrt{1 - k^2}$$

Now let Γ be the rectangular region of the T-plane shown in sketch (h), with vertices

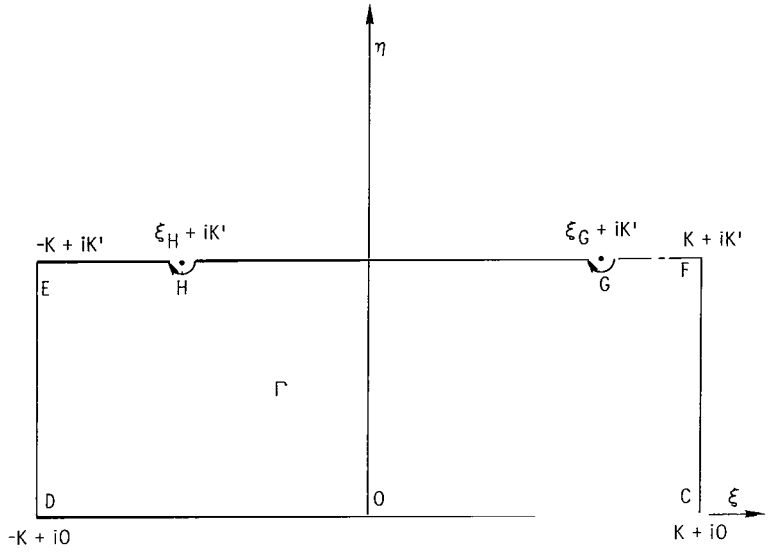

(h) Region Γ in T-plane.

at the points $-K + iK'$, $K + iK'$, $K + i0$ and $-K + i0$. The nozzle exit will be mapped onto the bottom side of the rectangle. The free streamlines will be mapped onto the vertical sides, and the ground and line of symmetry are mapped onto the top of the rectangle. The correspondence can be seen by comparing sketches (d) and (h).

Mapping Functions

Mapping function between ζ and T planes. - The function ζ: $\Gamma \rightarrow I$ will now be constructed. To accomplish this we will use the holomorphic function Ω studied in appendix A (see ref. 6) and defined on Γ by

$$\Omega(T;\ \xi_r, k) = \frac{\vartheta_4\left(\frac{\pi}{4K}(T - \xi_r)\middle|\frac{iK'}{2K}\right)}{\vartheta_4\left(\frac{\pi}{4K}(T + \xi_r - 2K)\middle|\frac{iK'}{2K}\right)} \qquad T \in \Gamma \tag{3}$$

The quantity $\vartheta_4(Z|\tau)$ is the fundamental Theta-function (See discussion in appendix A).

We will now demonstrate that the proper mapping function ζ is given by

$$\zeta(T) = V_o e^{i[(\pi/2)-\alpha]}\Omega(T;\ \xi_H, k)\sqrt{\Omega(T;\ \xi_G, k)} \qquad T \in \Gamma \tag{4}$$

First equation (A17a) shows that $\zeta(T) = 0$ only at the stagnation points G and H where $T = \xi_G + iK'$ and $\xi_H + iK'$, respectively. Equation (A18) shows that the arguments of both Ω functions in equation (4) are 0 along $\widehat{DC}$ since the Ω are positive and real on the real axis of the T-plane. Then

$$\arg \zeta(T) = \frac{\pi}{2} - \alpha \qquad \text{for} \quad T \in \widehat{DC}$$

which represents the nozzle cut in sketch (e). Equations (A20) and (A22) show that

$$|\zeta(T)| = V_o \qquad \text{for} \begin{cases} T \in \widehat{CF} \\ \\ T \in \widehat{ED} \end{cases}$$

which is the proper behavior along the circular hodograph of the free streamlines in sketch (e). Next equation (A24) shows that in traversing the points G and H along the

boundary of the rectangle Γ in a counterclockwise direction (i.e., along $\widehat{FGHE}$) the argument of $\zeta(T)$ decreases by $\pi/2$ at G and π at H, and is constant on the segments $\widehat{FG}$, $\widehat{GH}$ and $\widehat{HE}$. This agrees with the hodograph configuration in sketch e.

Finally, it follows by use of (A24) that $\arg \zeta(T) = (\pi/2) - \alpha + (\pi/2)\left[(\xi_H/K) + 1\right] + (\pi/4)\left[(\xi_0/K) + 1\right]$; $T \in \widehat{GF}$. On the hodograph of sketch (e) $\arg \zeta(T) = 3\pi/2$; $T \in \widehat{GF}$. The last two expressions will be compatible if we set

$$\left(\frac{\pi}{4} + \alpha\right) \frac{4K}{\pi} = \xi_G + 2\xi_H \tag{5}$$

This combined with the maximum modulus principle (ref. 5) shows that the function defined by equation (4) with the condition of equation (5) maps Γ onto I in such a way that the boundary of Γ is mapped onto the boundary of I.

Mapping function between W and T planes. - In order to complete the relation between ζ and W the function W that maps Γ onto J must be constructed. To accomplish this the intermediate t-plane shown in sketch (g) is utilized. An application of the Schwarz-Christoffel transformation (ref. 8) shows that the mapping that transforms the upper half of the t-plane onto the region J of the W-plane in the manner indicated in sketches (f) and (g) is defined by

$$\frac{dW}{dt} = iA_o \frac{(t - t_H)}{(1 - k^2t^2)\sqrt{1 - t^2}} \qquad ; \mathcal{I}m\, t > 0 \tag{6}$$

Now it is shown in reference 9 (p. 359) that the rectangle of sketch (h) is mapped onto the upper half t-plane of sketch (g) by

$$t = sn(T, k) \qquad T \in \Gamma \tag{7a}$$

where sn is the sine amplitude function. The inverse of this function is defined by

$$T = \int_0^t \frac{dt}{\sqrt{1 - t^2}\,\sqrt{1 - k^2t^2}} \tag{7b}$$

it is common to write sn T in place of sn(T, k) when the modulus k is not important to the discussion.

Using the relations (ref. 9)

$$\sqrt{1 - k^2t^2} = dn(T, k)$$

$$\sqrt{1 - t^2} = cn(T, k)$$

Equation (7b) can be written as

$$\frac{dt}{dT} = cn\ T\ dn\ T$$

At point H

$$t_H = sn\ T_H = sn(\xi_H + iK') = \frac{1}{k\ sn\ \xi_H}$$

Equation (6) can now be written in terms of the variable T

$$\frac{dW}{dT} = \frac{dW}{dt}\frac{dt}{dT} = iA_o \frac{sn\ T - sn\ T_H}{dn^2T\ cn\ T} cn\ T\ dn\ T = iA \frac{(k\ sn\ \xi_H\ sn\ T - 1)}{dn\ T} \qquad T \epsilon \Gamma \tag{8}$$

Upon integration equation (8) becomes

$$W = iA\left\{k\ sn\ \xi_H \int \frac{sn\ T\ dT}{dn\ T} dT - \int \frac{dT}{dn\ T} - \frac{C_o}{k'}\right\}$$

$$= -iA\left\{k\ sn\ \xi_H \int \frac{d(cn\ T)}{dn^2T} + \frac{1}{k'} \int dn(T + K)dT + \frac{C_o}{k'}\right\}$$

where the following identities (ref. 9) have been used

$$d(\text{cn } T) = -\text{sn } T \text{ dn } T \, dT$$

$$\text{dn}(T + K) = \frac{k'}{\text{dn } T}$$

Noting that (ref. 9)

$$\int \text{dn } T \, dT = \sin^{-1}(\text{sn } T) \equiv \text{am} T$$

$$\text{dn}^2 T = k'^2 + k^2 \, \text{cn}^2 T$$

we get

$$W = -iA\left\{k \, \text{sn } \xi_H \int \frac{d(\text{cn } T)}{k'^2 + k^2 \text{cn}^2 T} + \frac{1}{k'} \text{am}(T + K) + \frac{C_o}{k'}\right\}$$

$$= -\frac{iA}{k'}\left\{\text{sn } \xi_H \tan^{-1}\left(\frac{k}{k'} \text{cn } T\right) + \text{am}(T + K) + C_o\right\} \tag{9a}$$

An alternate form is

$$W = -\frac{iA}{k'}\left\{\text{sn } \xi_H \tan^{-1}\left(\frac{k}{k'} \text{cn } T\right) + \tan^{-1}(k' \text{ tn } T) + \frac{\pi}{2} + C_o\right\} \tag{9b}$$

where the relation (ref. 7) $\text{am}(T + K) = \tan^{-1}(k' \text{ tn} T) + (\pi/2)$ has been used.

Since the velocity potential is constant across the nozzle exit, the change in W(T) between the points D and C is equal to i times the change in the stream function between these points which in turn is equal to the net flow through the nozzle. Hence, if $\bar{V}_I$ is the average velocity at the nozzle exit and Δ is the nozzle width

$$i\bar{V}_I\Delta = i\psi(-K, 0) - i\psi(K, 0) = W(-K + i0) - W(K + i0)$$

Using the relations (ref. 7)

$$\text{cn}(-K) = \text{cn}K = 0$$

$$\text{am } 0 = 0$$

$$\text{am}(2K) = \pi$$

in equation (9a) gives

$$W(-K) = -\frac{iA}{k'} C_o$$

$$W(K) = -\frac{iA}{k'} (\pi + C_o)$$

so that

$$i\overline{V}_I \Delta = \frac{iA\pi}{k'}$$

Hence the constant A is related to the flow by

$$A = \frac{\overline{V}_I k' \Delta}{\pi} \tag{10}$$

As shown in sketch (d), the impingement on the plate causes the jet to divide; a portion of the net flow through the nozzle, designated by δ_R, flowing to the right and a portion δ_L to the left. The flow to the right must be equal to the jump in the imaginary part of W at the point E. In order to evaluate this jump notice that

$$\mathcal{I}m\ W(-K + i\eta) = \mathcal{I}m\, W(-K) = -\frac{A}{k'} C_o$$

$$\lim_{\eta \to K'} \mathcal{I}m\, W(-K + i\eta) = -\frac{A}{k'} C_o \tag{11}$$

On the other hand since

$$cn(\xi + iK') = -\frac{i}{k} \frac{dn\ \xi}{sn\ \xi}$$

$$sn(\xi + iK') = \frac{1}{k} \frac{1}{sn\ \xi}$$

$$tn(\xi + iK') = \frac{i}{dn\ \xi}$$

it follows from equation (9b) that

$$W(\xi + iK') = -\frac{iA}{k'}\left\{sn\ \xi_H \tan^{-1}\left(-\frac{i}{k'}\frac{dn\ \xi}{sn\ \xi}\right) + \tan^{-1}\left(\frac{ik'}{dn\ \xi}\right) + \frac{\pi}{2} + C_o\right\}$$

$$= \frac{A}{2k'}\left\{sn\ \xi_H \ln\left[\frac{k'sn\ \xi - dn\ \xi}{k'sn\ \xi + dn\ \xi}\right] + \ln\left[\frac{dn\ \xi + k'}{dn\ \xi - k'}\right] - i(\pi + 2C_o)\right\}$$

Since $k'^2sn^2\xi - dn^2\xi = -cn^2\xi$ we get

$$W(\xi + iK') = \frac{A}{2k'}\left\{sn\ \xi_H \ln\left[\frac{(k'sn\ \xi - dn\ \xi)^2}{k'^2sn^2\xi - dn^2\ \xi}\right] + \ln\left[\frac{dn\ \xi + k'}{dn\ \xi - k'}\right] - i(\pi + 2C_o)\right\}$$

$$= \frac{A}{2k'}\left\{sn\ \xi_H \ln(k'sn\ \xi - dn\xi)^2 + \ln\left(\frac{dn\ \xi + k'}{dn\ \xi - k'}\right) - sn\ \xi_H \ln(-cn^2\ \xi) - i(\pi + 2C_o)\right\}$$

$$= \frac{A}{2k'}\left\{sn\ \xi_H \ln(k'\ sn\ \xi - dn\ \xi)^2 - sn\ \xi_H \ln\ cn^2\ \xi \right.$$

$$\left. + \ln\left(\frac{dn\ \xi + k'}{dn\ \xi - k'}\right) - i(sn\ \xi_H\ \pi + \pi + 2C_o)\right\}$$

It is shown in reference 9 that $dn\ \xi$ is strictly greater than k' (i.e., never equal to k') for $-K < \xi < K$.

Also, keeping in mind that ξ is real, the imaginary part of W is

$$\mathcal{I}m\ W(\xi + iK') = -\frac{A\pi}{2k'}(1 + sn\ \xi_H) - \frac{AC_o}{k'}$$

Hence,

$$\lim_{\xi \to -K} \mathcal{I}m\ W(\xi + iK') = -\frac{A\pi}{2k'}(1 + sn\ \xi_H) - \frac{AC_o}{k'} \qquad (12)$$

Since the velocity at the point E must be V_o, it follows from equations (11) and (12) that if δ_R is the asymptotic height of the righthand free streamline above the ground sketch (d).

$$\delta_R V_o = \lim_{\eta \to K'} \mathcal{Im}\, W(-K + i\eta) - \lim_{\xi \to -K} \mathcal{Im}\, W(\xi + iK')$$

$$= -\frac{A}{k'} C_o + \frac{A\pi}{2k'} (1 + sn\ \xi_H) + \frac{AC_o}{k'} = \frac{A\pi}{2k'} (1 + sn\ \xi_H)$$

Inserting A from equation (10)

$$\frac{\delta_R}{\Delta} = \frac{\overline{V}_I}{V_o} \frac{1}{2} (1 + sn\ \xi_H) \tag{13}$$

As shown in sketch (d), δ_L is the width of the stream resulting from the flow to the left. Continuity requirements dictate that

$$\delta_R V_o + \delta_L V_o = \overline{V}_I \Delta$$

Hence, using equation (13)

$$\frac{\delta_L}{\Delta} = \frac{\overline{V}_I}{V_o} \frac{1}{2} (1 - sn\ \xi_H) \tag{14}$$

and

$$\frac{\delta_R}{\delta_L} = \frac{(1 + sn\ \xi_H)}{(1 - sn\ \xi_H)}$$

or

$$sn\ \xi_H = \frac{\dfrac{\delta_R}{\delta_L} - 1}{\dfrac{\delta_R}{\delta_L} + 1} \tag{15}$$

Determination of Flow Quantities

Integration to yield coordinates in physical plane. - Knowing the complex conjugate velocity ζ and the complex potential W as functions of the parametric variable T, the physical variable z can be found as a function of T by using equation (1). Carrying out the integration in the T-plane, instead of in the W-plane,

$$z = \int_{\xi_G + iK'}^{T} \frac{1}{\zeta} \frac{dW}{dT} dT \tag{16}$$

where the origin of the physical coordinate system has been chosen at the point G. After substituting equations (4), (8) and (10), equation (16) becomes

$$\frac{z}{\Delta} = \frac{k'}{\pi} \left(\frac{\overline{V}_I}{V_o} \right) e^{i\alpha} \int_{\xi_G + iK'}^{T} \frac{(k \operatorname{sn} \xi_H \operatorname{sn} T - 1) dT}{\operatorname{dn} T \, \Omega(T;\, \xi_H,\, k) \sqrt{\Omega(T;\, \xi_G,\, k)}} \tag{17}$$

Average velocity at nozzle exit. - In order to find an expression for $\overline{V}_I / V_o$ note that the nozzle lies between $T = -K + i0$ and $T = K + i0$, and therefore

$$z(-K) - z(K) = \Delta e^{i\alpha}$$

Using equation (17)

$$\frac{k'}{\pi} \left(\frac{\overline{V}_I}{V_o} \right) \int_{K}^{-K} \frac{(k \operatorname{sn} \xi_H \operatorname{sn} T - 1) dT}{\operatorname{dn} T \, \Omega(T;\, \xi_H,\, k) \sqrt{\Omega(T;\, \xi_G,\, k)}} = 1$$

The integration can be performed along the line $\widehat{DC}$. Therefore

$$\frac{\overline{V}_I}{V_o} = \left[\frac{k'}{\pi} \int_{-K}^{K} \frac{(1 - k \operatorname{sn} \xi_H \operatorname{sn} \xi) d\xi}{\operatorname{dn} \xi \, \Omega(\xi;\, \xi_H,\, k) \sqrt{\Omega(\xi;\, \xi_G,\, k)}} \right]^{-1} \tag{18}$$

Pressure coefficient. - The pressure coefficient C_p is defined as $[p(x, 0) - p_o]/1/2\ \rho V_o^2$. By use of Bernoulli's equation

$$C_p = 1 - \left[\frac{u(\xi, K')}{V_o}\right]^2 \tag{19}$$

where the velocity ratio and corresponding physical position along the ground are given by equation (B13).

Summary of Analytical Relations

For convenience the results of the ANALYSIS are now collected in one place

$$\operatorname{sn} \xi_H = \frac{\frac{\delta_R}{\delta_L} - 1}{\frac{\delta_R}{\delta_L} + 1} \tag{15}$$

$$\left(\frac{\pi}{4} + \alpha\right)\frac{4K}{\pi} = \xi_G + 2\xi_H \tag{5}$$

$$\Omega(T;\ \xi_r,\ k) = \frac{\vartheta_4\left(\frac{\pi}{4K}(T - \xi_r)\middle|\frac{iK'}{2K}\right)}{\vartheta_4\left(\frac{\pi}{4K}(T + \xi_r - 2K)\middle|\frac{iK'}{2K}\right)} \tag{3}$$

$$\frac{\zeta(T)}{V_o} = e^{i\left[(\pi/2)-\alpha\right]}\Omega(T;\ \xi_H,\ k)\sqrt{\Omega(T;\ \xi_G,\ k)} \tag{4}$$

$$\frac{W(T)}{V_o \Delta} = -\frac{i}{\pi}\left(\frac{\bar{V}_I}{V_o}\right)\left[\operatorname{sn} \xi_H \tan^{-1}\left(\frac{k}{k'}\operatorname{cn} T\right) + \operatorname{am}(T + K) + C_o\right] \tag{9a, 10}$$

$$\frac{z(T)}{\Delta} = \frac{k'}{\pi}\left(\frac{\bar{V}_I}{V_o}\right)e^{i\alpha}\int_{\xi_G + iK'}^{T} \frac{(k \operatorname{sn} \xi_H \operatorname{sn} T - 1)\,dT}{\operatorname{dn} T\ \Omega(T;\ \xi_H,\ k)\sqrt{\Omega(T;\ \xi_G, k)}} \tag{17}$$

$$\frac{\delta_R}{\Delta} = \frac{\bar{V}_I}{V_o} \frac{1}{2} (1 + \text{sn } \xi_H) \tag{13}$$

$$\frac{\bar{V}_I}{V_o} = \left[\frac{k'}{\pi} \int_{-K}^{K} \frac{(1 - k \text{ sn } \xi_H \text{sn } \xi) d\xi}{\text{dn } \xi \, \Omega(\xi;\ \xi_H,\ k) \sqrt{\Omega(\xi;\ \xi_G,\ k)}} \right]^{-1} \tag{18}$$

$$C_p = 1 - \left[\frac{u(\xi,\ K')}{V_o} \right]^2 \tag{19}$$

These expressions are further developed into working formulas in appendix B.

RESULTS AND DISCUSSION

The results that will be presented are the free streamlines, wall pressure coefficient, velocity distribution at the nozzle exit, and the ratio of the flow amounts to the right and left as a consequence of the jet impingement. These quantities will be presented in terms of three physical parameters, the tilt angle α of the nozzle, the horizontal distance of the nozzle center from the plane of symmetry between the two jets, and the vertical height of the center of the nozzle exit plane above the ground. The coordinates to the nozzle center divided by the nozzle width Δ, are designated by X_N and Y_N.

The angle α appears explicitly in the analysis and hence could be directly specified as an input variable in the computer program used to evaluate the anlytical expressions. The nozzle position however has to be determined from the calculations and the following procedure was used. A value was chosen for δ_L/δ_R and for k, each being between 0 and 1. Then ξ_H can be found from equation (15). For a given α, ξ_G is found from equation (5), the value of K having been found as the complete elliptic integral, equation (2). The average velocity from the nozzle is computed from equation (18) with the ϑ_4 in the Ω functions found from equation (A1). The width of the flow stream to the right δ_R/Δ is then computed from equation (13), and δ_L/Δ is found by dividing δ_R/Δ by the specified ratio δ_L/δ_R.

The contours of the free streamlines were obtained from the working formulas (B14) and (B15) developed in appendix B. This gives the free streamline coordinates relative to the points C and D in sketch (d). Since δ_L is known, it is added to the horizontal distance between C and F on the left free streamline to horizontally locate point C. The vertical position of C is found from δ_R, the streamline height between E and D, and the

nozzle tilt angle. In this manner the nozzle position is found in terms of the variables α, δ_L/δ_R and k which are the convenient input quantities in the computer program.

The relation between δ_L/δ_R, k, and the dimensionless coordinates X_N, Y_N (the location of the center of the nozzle exit plane) for various nozzle tilt angles is shown in figures 1(a) to (e). These plots are helpful for performing computations of the flow configurations in addition to those that will be presented here since they provide the input parameters δ_L/δ_R and k for a desired nozzle position. The main utility of these figures is that the ratio δ_L/δ_R can be readily found for a given nozzle position and tilt angle. From δ_L/δ_R the fraction of the flow that travels back up the y-axis is found as

$$\frac{\delta_L}{\delta_L + \delta_R} = \frac{\dfrac{\delta_L}{\delta_R}}{\dfrac{\delta_L}{\delta_R} + 1}$$

In figure 1(a), which is for 0^o nozzle tilt, as the spacing X_N between nozzles is increased, the ratio δ_L/δ_R approaches 1. For large X_N the two jets have little influence on each other and the flow from each jet divides equally. When the nozzles are tilted, for a fixed Y_N the δ_L/δ_R approaches a constant value less than 1 as the spacing X_N is increased. The limiting values of δ_L/δ_R for large X_N are shown on the curves; for example, for $\alpha = 15^o$ and $Y_N = 1.5$, $\delta_L/\delta_R = 0.588$ for all $X_N > 2$.

The velocity distribution along the nozzle exit plane, and the velocity along the ground were computed from equations (B12) and (B13). The velocity variation along the ground was inserted into equation (19) to obtain the pressure coefficient. The free streamlines, velocity distribution across the nozzle exit plane, and the pressure coefficient along the ground are plotted in figures 2 to 6.

Each of figures 2 to 6 is for a fixed tilt angle; 0^o, 5^o, 10^o, 15^o, or 20^o. The (a) and (b) parts of each figure are respectively for spacings $X_N = 1$ and 2, and each part has the two vertical positions $Y_N = 1$ and 2.

An examination of the figures reveals a number of specific characteristics of the flow. When the nozzle is near the ground, the reaction against the ground causes the velocity distribution across the nozzle to be nonuniform and decreases the flow out of the nozzle. Raising and/or tilting the nozzle decreases the interaction with the ground and causes the velocity distribution to become more uniform. The nozzle exit velocity is also influenced to a small extent by the spacing between the nozzles; the velocity distribution being more uniform as X_N is increased.

The effect of nozzle tilt on the amount of flow back along the y-axis is shown in figure 7. Figures 7(a) and (b), respectively, show the results for 4 nozzle tilt angles at the fixed nozzle position $X_N = 1$, $Y_N = 2$, and 3 tilt angles for $X_N = 2$, $Y_N = 2$. In figure 7(b) the back flow decreases with increasing tilt angle. This is the behavior that would be expected from intuition and does occur for most nozzle positions. Figure 7(a) for a smaller X_N shows the effect of a more complex interaction of the two jets. In this instance as the tilt increases, the back flow increases until $\alpha = 23^o$; then a further increase in α causes the back flow to decrease. This is shown more explitly in figure 8, where δ_L/δ_R has been cross plotted as a function of tilt angle.

CONCLUDING REMARKS

Conformal mapping was used to obtain the configuration of flow from two slot nozzles tilted with respect to the ground. The condition imposed is that the flow leaves each nozzle in a direction perpendicular to the nozzle exit plane. The flow strikes the ground and a portion flows back upward along the plane of symmetry between the nozzles. The interaction of the flow from each nozzle with the ground and with the flow from the other nozzle causes the velocity distribution leaving the nozzles to the nonuniform.

The free streamlines are given for nozzle tilt angles up to 20^o; for VTOL application only small tilt angles would be of interest. At most nozzle positions, the back flow between the nozzles decreased with increasing tilt angle. For small spacings between the nozzles an interesting effect was found. Tilting the nozzles increased the back flow until a maximum was reached; then with larger tilting the back flow began to decrease.

Lewis Research Center,
National Aeronautics and Space Administration,
Cleveland, Ohio, October 30, 1968,
129-01-07-07-22.

REFERENCES

1. Gardon, Robert; and Akfirat, J. Cahit: Heat Transfer Characteristics of Impinging Two-Dimensional Air Jets. J. Heat Transfer, vol. 88, no. 1, Feb. 1966, pp. 101-108.

2. Gedney, Richard T.; and Siegel, Robert: Inviscid Flow Analysis of Two Parallel Slot Jets Impinging Normally on a Surface. NASA TN D-4957, 1968.

3. Spooner, S. H.: The V/STOL Aircraft Environment. Paper No. 68-GT-40, ASME, Mar. 1968.

4. Williams, John ; and Wood, Maurice N.: Aerodynamic Interference Effects with Jet-Lift V/STOL Aircraft under Static and Forward-Speed Conditions. Zeit. für Flug., vol. 15, no. 7, July 1967, pp. 237-256.

5. Kemp, E. D. G.: Studies of Exhaust Gas Recirculation for VTOL Aircraft. Paper No. 67-439, AIAA, July 1967.

6. Birkhoff, Garrett; and Zarantonello, E. H.: Jets, Wakes, and Cavities. Academic Press, 1957.

7. Byrd, P. F.; and Friedman, M. D.: Handbook of Elliptic Integrals for Engineers and Physicists. Springer-Verlag, Berlin, 1954.

8. Churchill, Ruel V.: Complex Variables and Applications. Second ed., McGraw-Hill Book Co., Inc., 1960.

9. Moretti, Gino: Functions of a Complex Variable. Prentice-Hall, Inc., 1964.

10. Whittaker, Edmund T.; and Watson, G. N.: A Course of Modern Analysis. Fourth ed., Cambridge Univ. Press, 1927.

11. Rainville, Earl D.: Special Functions. The Macmillan Co., 1960.

APPENDIX A

PROPERTIES OF FUNCTION Ω

The properties of the function Ω will be derived in this appendix. To accomplish this it will be useful to list some properties of the Theta-functions. The Jacobi notation as modified by Tannery and Molk for the Theta-functions will be used here. This is the same notation as used in reference 10. There are four types of Theta-functions denoted by ϑ_1, ϑ_2, ϑ_3, ϑ_4. The functions ϑ_1, ϑ_2 and ϑ_3 are defined in terms of ϑ_4. For any complex constant τ such that $\mathcal{I}m\,\tau > 0$, the function ϑ_4 is defined by

$$\vartheta_4(z\,|\,\tau) = 1 + 2\sum_{n=1}^{\infty}(-1)^n e^{i\pi n^2\tau}\cos 2nz \tag{A1}$$

for every complex number $z = x + iy$. It is shown in reference 10 that the series (A1) is absolutely convergent in the whole complex plane and that ϑ_4 is an entire function (holomorphic in the whole complex plane). It is also shown in references 10 and 11 that the zeros of ϑ_4 are all simple. Thus, if z_o is a zero of ϑ_4

$$\vartheta_4(z\,|\,\tau) \sim (z - z_o) \qquad \text{for } z \text{ near } z_o \tag{A2}$$

The zeros of ϑ_4 are the points $z_{m,n}$ given by (ref. 11)

$$z_{m,n} = \frac{1}{2}\pi\tau + m\pi + n\pi\tau \qquad ;\ m, n = 0, \pm 1, \pm 2, \ldots \tag{A3}$$

It is seen from the behavior of $\cos 2nz$ in equation (A1) that

$$\vartheta_4(z \pm \pi\,|\,\tau) = \vartheta_4(z\,|\,\tau) \tag{A4}$$

$$\vartheta_4(-z\,|\,\tau) = \vartheta_4(z\,|\,\tau) \tag{A5}$$

The remaining Theta-functions are now defined in terms of ϑ_4 by (ref. 10)

$$\vartheta_1(z\,|\,\tau) = -ie^{iz+(1/4)\pi i\tau}\vartheta_4\left(z + \frac{1}{2}\pi\tau\,\middle|\,\tau\right) \tag{A6}$$

$$\vartheta_2(z\,|\,\tau) = \vartheta_1\left(z + \frac{1}{2}\,\pi\,|\,\tau\right) \tag{A7}$$

$$\vartheta_3(z\,|\,\tau) = \vartheta_4\left(z + \frac{1}{2}\,\pi\,|\,\tau\right) \tag{A8}$$

By substituting the definition (A1) into the definitions (A6) to (A8) these Theta-functions are given by

$$\vartheta_1(z\,|\,\tau) = 2\sum_{n=0}^{\infty}(-1)^n e^{i\pi\tau[n+(1/2)]^2}\sin(2n+1)z \tag{A9}$$

$$\vartheta_2(z|\,\tau) = 2\sum_{n=0}^{\infty} e^{i\pi\tau[n+(1/2)]^2}\cos(2n+1)z \tag{A10}$$

$$\vartheta_3(z\,|\,\tau) = 1 + 2\sum_{n=1}^{\infty} e^{i\pi\tau n^2}\cos 2nz \tag{A11}$$

From the behavior of the sine function together with eq. (A9) it can be concluded that

$$\vartheta_1(-z\,|\,\tau) = -\vartheta_1(z\,|\,\tau) \tag{A12}$$

For the problem analyzed in this report the argument τ in the Theta-functions is always a pure imaginary number, and it will be assumed that τ is pure imaginary in the discussion that follows. In this instance their definitions show that the Theta-functions are all real when z is real; that is, along the real axis of the z-plane. It follows from (A3) that there are no zeros of ϑ_4 on the real axis, and hence it follows that ϑ_4 cannot change sign there. From (A1) at $z = x + i0 = \pi/2$

$$\vartheta_4\left(\frac{\pi}{2}\,\middle|\,\tau\right) = 1 + 2\sum_{n=1}^{\infty} e^{i\pi n^2\tau} > 0$$

Since ϑ_4 cannot change sign on the real axis

$$\vartheta_4(x|\tau) > 0 \qquad -\infty < x < +\infty \tag{A13}$$

To examine the complex conjugate of ϑ_4 and ϑ_3 note that $\cos z = \cos x \cosh y - i \sin x \sinh y$, which yields

$$(\cos z)^* = \cos z^*$$

Then from equations (A1) and (A11)

$$\left.\begin{aligned} \left[\vartheta_4(z|\tau)\right]^* &= \vartheta_4(z^*|\tau) \\ \left[\vartheta_3(z|\tau)\right]^* &= \vartheta_3(z^*|\tau) \end{aligned}\right\} \tag{A14}$$

Now let Γ be the closed rectangle in the complex T-plane shown in sketch (i)

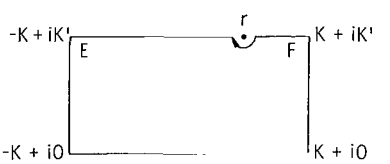

(i) Region Γ in T-plane showing boundary point r used in derivation.

with vertices at the points $-K + iK'$, $K + iK'$, K and $-K$. For any real number ξ_r such that $-K < \xi_r < K$, Ω is the complex function defined on Γ by

$$\Omega(T; \xi_r, k) = \frac{\vartheta_4\left(\frac{\pi}{4K}(T - \xi_r) \,\middle|\, \frac{iK'}{2K}\right)}{\vartheta_4\left(\frac{\pi}{4K}(T + \xi_r - 2K) \,\middle|\, \frac{iK'}{2K}\right)} \qquad T \in \Gamma \tag{A15}$$

which is equation (3) in the main text.

Since ϑ_4 is an entire function and has simple isolated zeros, it is clear that Ω is meromorphic in the interior of Γ (i.e., it can have only isolated poles in Γ which would occur when ϑ_4 in the denominator of (A15) is zero). In fact the formula (A15) can be used to extend Ω to a meromorphic function in the entire T-plane. The function Ω can have only simple poles located at the points T for which

$$\vartheta_4\left(\frac{\pi}{4K}(T + \xi_r - 2K)\middle|\frac{iK'}{2K}\right) = 0$$

Equation (A3) shows that these points are given by

$$T = -\xi_r + 2(1 + 2m)K + i(1 + 2n)K' \quad ; \; m, \; n = 0, \pm 1, \pm 2, \ldots \tag{A16}$$

However, for all $T \epsilon \Gamma$ (and recalling that $|\xi_r| < |K|$) it must be true that $|\xi + \xi_r| < 2K$, and so equation (A16) shows that Ω has no poles in Γ or on the boundary of Γ. Thus, Ω is holomorphic in the interior of Γ, and since the poles are isolated, Ω can be extended to a holomorphic function in some open set which contains Γ. This shows that Ω is continuous on the boundary of Γ.

The zeros of Ω are located at the points T for which

$$\vartheta_4\left(\frac{\pi}{4K}(T - \xi_r)\middle|\frac{iK'}{2K}\right) = 0$$

Equation (A3) shows that these points are given by

$$T = \xi_r + 4mK + i(1 + 2n)K' \quad ; \; m, \; n = 0, \pm 1, \pm 2, \ldots \tag{A17a}$$

Since $|\xi - \xi_r| < 2K$ and $0 \leq \eta \leq iK'$ for $T \epsilon \Gamma$, the only zero of Ω on Γ is at a boundary point on the upper side of Γ given by ($m = n = 0$)

$$T = \xi_r + iK' \tag{A17b}$$

and this must be a simple zero of Ω. Thus, from equation (A2)

$$\Omega(T; \xi_r, k) \sim (T - \xi_r - iK') \text{ for } T \text{ near } \xi_r + iK'$$

Now the behavior of Ω will be examined on the sides of the rectangle Γ. Equation (A13) shows that on the bottom side of Γ which lies on the real axis of the T-plane,

$$\Omega(T; \xi_r, k) > 0 \qquad T \in \widehat{DC} \tag{A18}$$

Along the right side of Γ it follows by use of equation (A5) that

$$\Omega(i\eta + K;\ \xi_r,\ k) = \frac{\vartheta_4\left(\frac{\pi}{4K}(K - \xi_r + i\eta)\,\middle|\,\frac{iK'}{2K}\right)}{\vartheta_4\left(\frac{\pi}{4K}(K - \xi_r - i\eta)\,\middle|\,\frac{iK'}{2K}\right)} = \frac{\vartheta_4\left(\frac{\pi}{4K}(K - \xi_r + i\eta)\,\middle|\,\frac{iK'}{2K}\right)}{\vartheta_4\left(\frac{\pi}{4K}(K - \xi_r + i\eta)^*\,\middle|\,\frac{iK'}{2K}\right)} \tag{A19}$$

Then by applying equation (A14)

$$\Omega(i\eta + K;\ \xi_r,\ k) = \frac{\vartheta_4\left(\frac{\pi}{4K}(K - \xi_r + i\eta)\,\middle|\,\frac{iK'}{2K}\right)}{\left[\vartheta_4\left(\frac{\pi}{4K}(K - \xi_r + i\eta)\,\middle|\,\frac{iK'}{2K}\right)\right]^*}$$

This shows that along the right side $\widehat{CF}$ of the rectangle Γ

$$\left|\,\Omega(T;\ \xi_r,\ k)\,\right| = 1 \qquad \text{for } T \in \widehat{CF} \tag{A20}$$

Now examine Ω on the left side of Γ where $T = i\eta - K$. By applying equations (A4) and (A5)

$$\Omega(i\eta - K;\ \xi_r,\ k) = \frac{\vartheta_4\left(\frac{\pi}{4K}(\xi_r + K - i\eta)\,\middle|\,\frac{iK'}{2K}\right)}{\vartheta_4\left(\frac{\pi}{4K}(\xi_r + K + i\eta)\,\middle|\,\frac{iK'}{2K}\right)} = \frac{\vartheta_4\left(\frac{\pi}{4K}(\xi_r + K + i\eta)^*\,\middle|\,\frac{iK'}{2K}\right)}{\vartheta_4\left(\frac{\pi}{4K}(\xi_r + K + i\eta)\,\middle|\,\frac{iK'}{2K}\right)} \tag{A21}$$

Then by applying equation (A14)

$$\Omega(i\eta - K;\ \xi_r,\ k) = \frac{\left[\vartheta_4\left(\frac{\pi}{4K}(\xi_r + K + i\eta)\,\middle|\,\frac{iK'}{2K}\right)\right]^*}{\vartheta_4\left(\frac{\pi}{4K}(\xi_r + K + i\eta)\,\middle|\,\frac{iK'}{2K}\right)}$$

Hence,

$$\left|\,\Omega(T;\ \xi_r,\ k)\,\right| = 1 \qquad \text{for } T \in \widehat{DE} \tag{A22}$$

On the top side of Γ, $T = \xi + iK'$. From equations (A15) and (A6) it follows that

$$\Omega(\xi + iK';\ \xi_r,\ k) = -\frac{\vartheta_4\left(\frac{\pi}{4K}(\xi - \xi_r) + \frac{\pi}{2}\frac{iK'}{2K}\,\middle|\,\frac{iK'}{2K}\right)}{\vartheta_4\left(\frac{\pi}{4K}(\xi + \xi_r - 2K) + \frac{\pi}{2}\frac{iK'}{2K}\,\middle|\,\frac{iK'}{2K}\right)}$$

$$= e^{i(\pi/2)[(\xi_r/K)-1]}\ \frac{\vartheta_1\left(\frac{\pi}{4K}(\xi - \xi_r)\,\middle|\,\frac{iK'}{2K}\right)}{\vartheta_1\left(\frac{\pi}{4K}(\xi + \xi_r - 2K)\,\middle|\,\frac{iK'}{2K}\right)} \qquad \text{(A23)}$$

Since $\left(\frac{\pi}{4K}\right)(\xi - \xi_r)$ and $\left(\frac{\pi}{4K}\right)(\xi + \xi_r - 2K)$ are real, we see that $\vartheta_1\left(\frac{\pi}{4K}(\xi - \xi_r)\,\middle|\,\frac{iK'}{2K}\right)$ and $\vartheta_1\left(\frac{\pi}{4K}(\xi + \xi_r - 2K)\,\middle|\,\frac{iK'}{2K}\right)$ are real. Hence the argument of $\Omega(\xi + iK';\ \xi_r,\ k)$ is either equal to or can differ from the argument in the exponent, $\frac{\pi}{2}\left(\frac{\xi_r}{K} - 1\right)$, only by π depending on whether or not the ratios of the ϑ_1's is a positive or negative number. Equation (A17a) shows that in traversing the point $\xi_r + iK'$ along the contour $\widehat{FrE}$ in a counter-clockwise direction (as shown in sketch (i) and illustrated at the points $\xi_G + iK'$ and $\xi_H + iK'$ in sketch (h)) the argument of Ω must decrease by π. Since $\xi_r + iK'$ is the only zero of Ω on Γ, this is the only point of $\widehat{FrE}$ where the argument of Ω can change. Hence, the argument of Ω is constant on $\widehat{Fr}$ and on $\widehat{rE}$. Letting $\xi = K$ in (A23) gives

$$\Omega(K + iK';\ \xi_r,\ k) = e^{i(\pi/2)[(\xi_r/K)-1]}\ \frac{\vartheta_1\left(\frac{\pi}{4K}(K - \xi_r)\,\middle|\,\frac{iK'}{2K}\right)}{\vartheta_1\left(\frac{\pi}{4K}(\xi_r - K)\,\middle|\,\frac{iK'}{2K}\right)}$$

Using equation (A12) this becomes

$$\Omega(K + iK';\ \xi_r,\ k) = -e^{i(\pi/2)[(\xi_r/K)-1]} = e^{i(\pi/2)[(\xi_r/K) + 1]}$$

Thus,

$$\arg \Omega(T;\ \xi_r,\ k) = \begin{cases} \frac{\pi}{2}\left(\frac{\xi_r}{K} + 1\right) & ;T \in \widehat{Fr} \\ \frac{\pi}{2}\left(\frac{\xi_r}{K} - 1\right) & ;T \in \widehat{rE} \end{cases} \tag{A24}$$

In summary then we have shown that Ω is holomorphic on the interior of Γ and continuing on its boundaries. It has modulus of 1 on the vertical sides of Γ, and is positive on the bottom side of Γ. The argument of $\Omega(T;\ \xi_r,\ k)$ on the top side of Γ is equal to $(\pi/2)[(\xi_r/K) + 1]$ for $\xi > \xi_r$ and $(\pi/2)[(\xi_r/K) - 1]$ for $\xi < \xi_r$.

APPENDIX B

WORKING FORMULAS FOR COMPUTING FLOW PATTERN

In this appendix equations (4) and (17) will be rewritten in various forms which are convenient for computing the velocities on, and the positions of, the various boundaries of the flow.

It will be convenient to make the following definitions

$$\xi^+ = \frac{\pi}{4K}(K - \xi), \quad \xi_r^+ = \frac{\pi}{4K}(K - \xi_r), \quad \eta^+ = \frac{\pi}{4K}\eta, \quad \tau^+ = \frac{iK'}{2K} \tag{B1}$$

$$R_r^{(4)}(\xi) = \frac{\vartheta_4(\xi^+ - \xi_r^+ | \tau^+)}{\vartheta_4(\xi^+ + \xi_r^+ | \tau^+)} \tag{B2}$$

$$R_r^{(1)}(\xi) = \frac{\vartheta_1(\xi^+ - \xi_r^+ | \tau^+)}{\vartheta_1(\xi^+ + \xi_r^+ | \tau^+)} \tag{B3}$$

$$e^{iQ_r^{(4)}(\eta)} = \frac{\vartheta_4(\xi_r^+ + i\eta^+ | \tau^+)}{\vartheta_4(\xi_r^+ - i\eta^+ | \tau^+)} \tag{B4}$$

$$e^{iQ_r^{(3)}(\eta)} = \frac{\vartheta_3(\xi_r^+ + i\eta^+ | \tau^+)}{\vartheta_3(\xi_r^+ - i\eta^+ | \tau^+)} \tag{B5}$$

Equation (A13) shows that $R_r^{(4)}(\xi)$ is real and positive, and equation (A9) shows that $R_r^{(1)}(\xi)$ is real. Equations (A14) show that the ratios on the right side of equations (B4) and (B5) each have a modulus of 1; hence, $Q_r^{(4)}(\eta)$ and $Q_r^{(3)}(\eta)$ are real.

The function Ω defined in equation (3) can then be evaluated along the sides of Γ, corresponding to the boundaries of the flow, by use of the functions R and Q. It follows from the definition of Ω and equation (A5) that

$$\Omega(\xi;\ \xi_r,\ k) = R_r^{(4)}(\xi) \tag{B6}$$

Equations (A12) and (A23) show that

$$\Omega(\xi + iK';\ \xi_r,\ k) = e^{i\left[(\xi_r/K)-1\right](\pi/2)} R_r^{(1)}(\xi) \tag{B7}$$

Equation (A19) shows that

$$\Omega(K + i\eta;\ \xi_r,\ k) = e^{iQ_r^{(4)}(\eta)} \tag{B8}$$

Equations (A21), (A5), and (A8) show that

$$\Omega(-K + i\eta;\ \xi_r,\ k) = e^{iQ_r^{(3)}(\eta)} \tag{B9}$$

To put equation (17) in a form suitable for numerical computation purposes, it is necessary to express $(k\ sn\ \xi_H\ sn\ T - 1)/dn\ T$ in terms of real quantities when T is complex. The following relations are deduced in reference 9:

$$sn(\pm K + i\eta) = \pm\, cn(i\eta)/dn(i\eta)$$

$$dn(\pm K + i\eta) = k'/dn(i\eta)$$

$$dn(i\eta,\ k) = dn(\eta,\ k')/cn(\eta,\ k')$$

$$cn(i\eta,\ k) = 1/cn(\eta, k')$$

It follows that

$$sn(\pm K + i\eta,\ k) = \pm 1/dn(\eta,\ k')$$

$$dn(\pm K + i\eta,\ k) = k'\ cn(\eta,\ k')/dn(\eta,\ k')$$

$$\frac{k\ sn(\xi_H, k)sn(\pm K + i\eta,\ k) - 1}{dn(\pm K + i\eta,\ k)} = -\frac{1}{k'}\,\frac{dn(\eta, k') \mp k\ sn(\xi_H, k)}{cn(\eta,\ k')} \tag{B10}$$

Since (ref. 9)

$$sn(\xi + iK') = 1/k\ sn\ \xi$$

$$dn(\xi + iK') = -i\ cn\ \xi / sn\ \xi$$

it follows that

$$\frac{k\ sn\ \xi_H\ sn(\xi + iK') - 1}{dn(\xi + iK')} = -i\ \frac{(sn\ \xi - sn\ \xi_H)}{cn\ \xi} \tag{B11}$$

Using equations (B6) to (B11) and equation (5) in equations (4) and (17) shows after the obvious deformations of the path of integrations:

Positions and corresponding velocity along nozzle exit:

$$\left.\begin{aligned} \frac{z(-K) - z(\xi)}{\Delta} &= \left(\frac{\bar{V}_I}{V_o}\right)\frac{k'}{\pi}\int_{-K}^{\xi} \frac{1 - k\ sn(\xi_H, k)sn(\xi, k)}{dn(\xi, k)R_H^{(4)}(\xi)\sqrt{R_G^{(4)}(\xi)}}\,d\xi \\ \frac{|\zeta(\xi)|}{V_o} &= R_H^{(4)}(\xi)\ \sqrt{R_G^{(4)}(\xi)} \end{aligned}\right\} -K \le \xi \le K \tag{B12}$$

Position and corresponding velocity along the ground:

$$\left.\begin{aligned} \frac{x(\xi, K')}{\Delta} &= \left(\frac{\bar{V}_I}{V_o}\right)\frac{k'}{\pi}\int_{\xi_G}^{\xi} \frac{sn(\xi, k) - sn(\xi_H, k)}{cn(\xi, k)R_H^{(1)}(\xi)\sqrt{R_G^{(1)}(\xi)}}\,d\xi \\ \frac{u(\xi, K')}{V_o} &= R_H^{(1)}(\xi)\ \sqrt{R_G^{(1)}(\xi)} \end{aligned}\right\} -K \le \xi \le \xi_G \tag{B13}$$

Location of free streamlines:

$$\left.\begin{aligned} \frac{x(-K,\eta) - x(-K, 0)}{\Delta} &= \frac{1}{\pi}\left(\frac{\bar{V}_I}{V_o}\right)\int_0^{\eta} \frac{\left[dn(\eta, k') + k\ sn(\xi_H, k)\right]}{cn(\eta, k')}\ \cos\left[\frac{\pi}{2} - \alpha + Q_H^{(3)}(\eta) + \frac{1}{2}Q_G^{(3)}(\eta)\right]d\eta \\ \frac{y(-K,\eta) - y(-K, 0)}{\Delta} &= -\frac{1}{\pi}\left(\frac{\bar{V}_I}{V_o}\right)\int_0^{\eta} \frac{\left[dn(\eta, k') + ksn(\xi_H, k)\right]}{cn(\eta, k')}\ \sin\left[\frac{\pi}{2} - \alpha + Q_H^{(3)}(\eta) + \frac{1}{2}Q_G^{(3)}(\eta)\right]d\eta \end{aligned}\right\} \tag{B14}$$

$$\left.\begin{aligned}
\frac{x(K,\eta) - x(K,0)}{\Delta} &= \frac{1}{\pi}\left(\frac{\bar{V}_I}{V_o}\right)\int_0^{\eta} \frac{\left[dn(\eta,\ k') - k\ sn(\xi_H,\ k)\right]}{cn(\eta,\ k')} \cos\left[\frac{\pi}{2} - \alpha + Q_H^{(4)}(\eta) + \frac{1}{2}Q_G^{(4)}(\eta)\right]d\eta \\
\frac{y(K,\eta) - y(K,0)}{\Delta} &= -\frac{1}{\pi}\left(\frac{\bar{V}_I}{V_o}\right)\int_0^{\eta} \frac{\left[dn(\eta,\ k') - k\ sn(\xi_H,\ k)\right]}{cn(\eta,\ k')} \sin\left[\frac{\pi}{2} - \alpha + Q_H^{(4)}(\eta) + \frac{1}{2}Q_G^{(4)}(\eta)\right]d\eta
\end{aligned}\right\}$$

$$\text{where } 0 \leq \eta \leq K' \tag{B15}$$

The following quantities are useful for the computation of $Q_r^{(4)}$ and $Q_r^{(3)}$

$$\left.\begin{aligned}
A_r^{(4)}(\eta^+) &= 1 + 2\sum_{n=1}^{\infty}(-1)^n q^{n^2}\cos(2n\xi_r^+)\cosh(2n\eta^+) \\
B_r^{(4)}(\eta^+) &= -2\sum_{n=1}^{\infty}(-1)^n q^{n^2}\sin(2n\xi_r^+)\sinh(2n\eta^+) \\
A_r^{(3)}(\eta^+) &= 1 + 2\sum_{n=1}^{\infty} q^{n^2}\cos(2n\xi_r^+)\cosh(2n\eta^+) \\
B_r^{(3)}(\eta^+) &= -2\sum_{n=1}^{\infty} q^{n^2}\sin(2n\xi_r^+)\sinh(2n\eta^+) \\
&\text{where } q = e^{-(\pi/2)(K'/K)}
\end{aligned}\right\} \tag{B16}$$

Using the relation

$$\cos(x + iy) = \cos x \cosh y - i \sin x \sinh y$$

substituting equations (A1) and (A11) in definitions (B4) and (B5), respectively, and taking real parts yields

$$\cos\left[Q_r^{(4)}(\eta)\right] = \frac{\left[A_r^{(4)}(\eta^+)\right]^2 - \left[B_r^{(4)}(\eta^+)\right]^2}{\left[A_r^{(4)}(\eta^+)\right]^2 + \left[B_r^{(4)}(\eta^+)\right]^2}$$

$$\cos\left[Q_r^{(3)}(\eta)\right] = \frac{\left[A_r^{(3)}(\eta^+)\right]^2 - \left[B_r^{(3)}(\eta^+)\right]^2}{\left[A_r^{(3)}(\eta^+)\right]^2 + \left[B_r^{(3)}(\eta^+)\right]^2} \qquad \text{(B17)}$$

$Q_r^{(4)}$ must always be taken in the first and second quadrants and $Q_r^{(3)}$ must always be taken in the third and fourth quadrants.

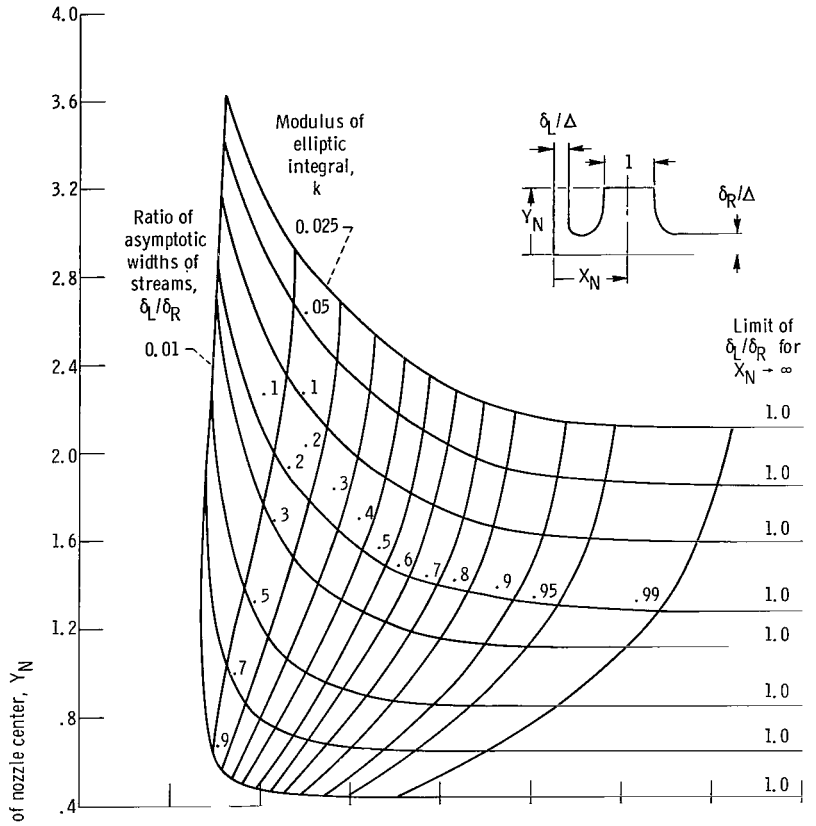

(a) Tilt angle, 0°.

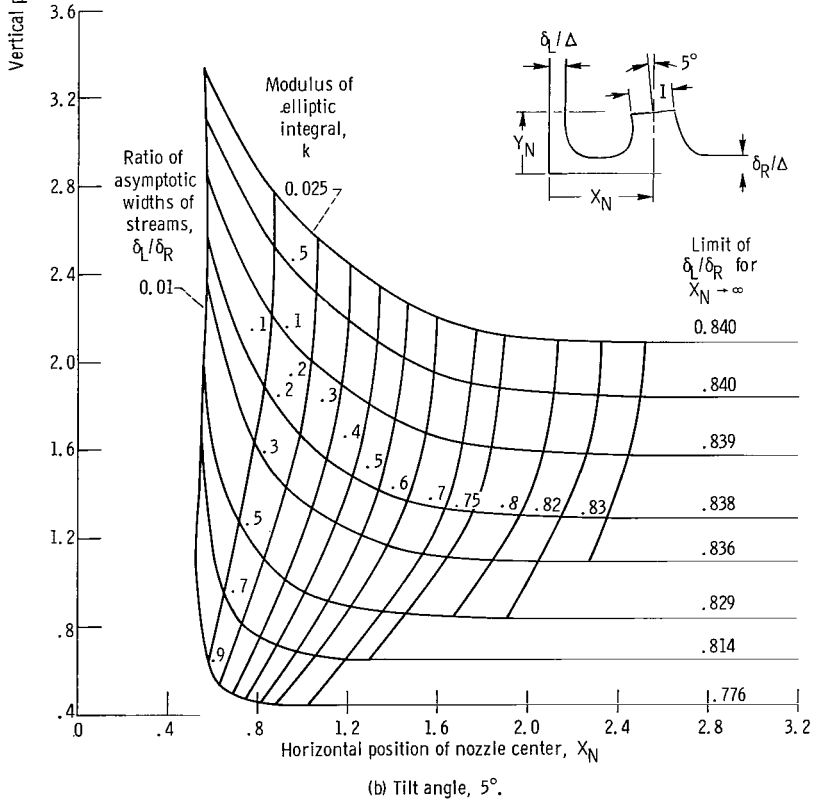

(b) Tilt angle, 5°.

Figure 1. - Ratio of flows to left and right as function of nozzle position.

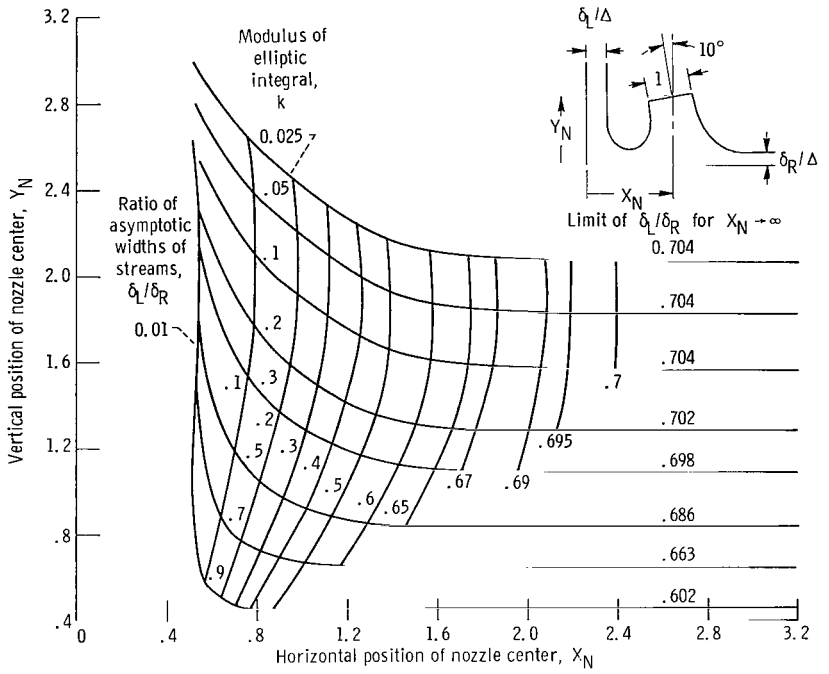

(c) Tilt angle, 10°.

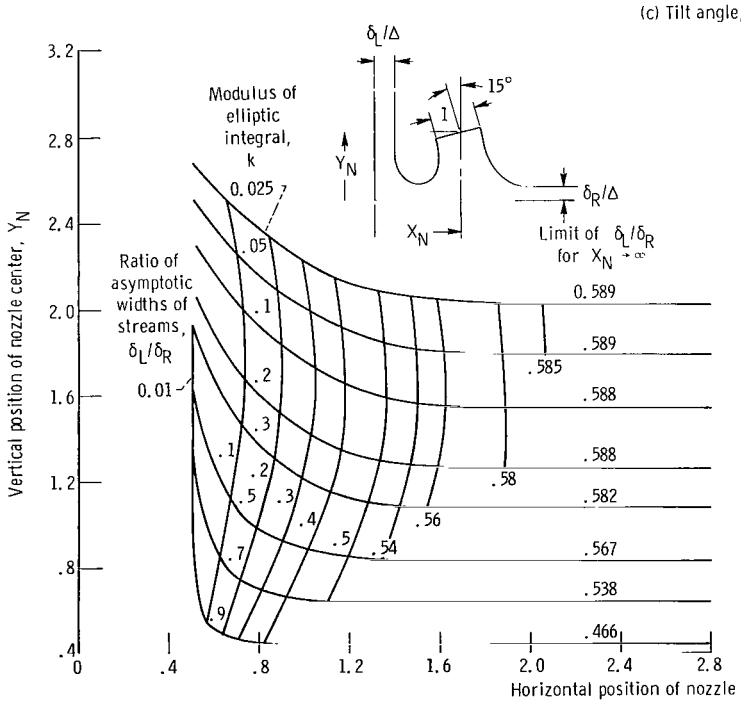

(d) Tilt angle, 15°.

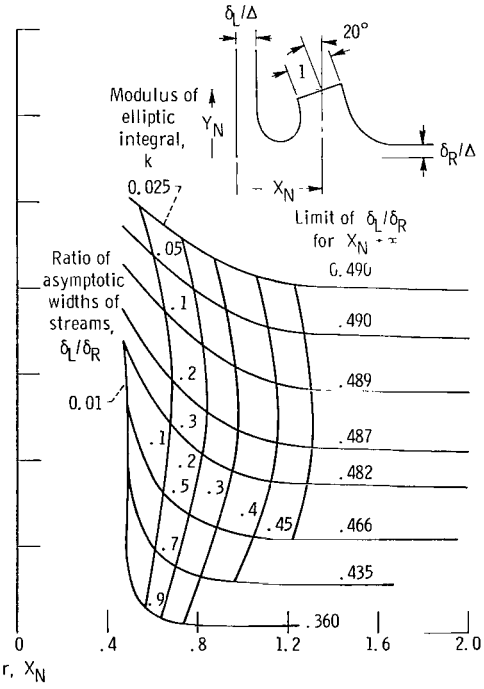

(e) Tilt angle, 20°.

Figure 1. - Concluded.

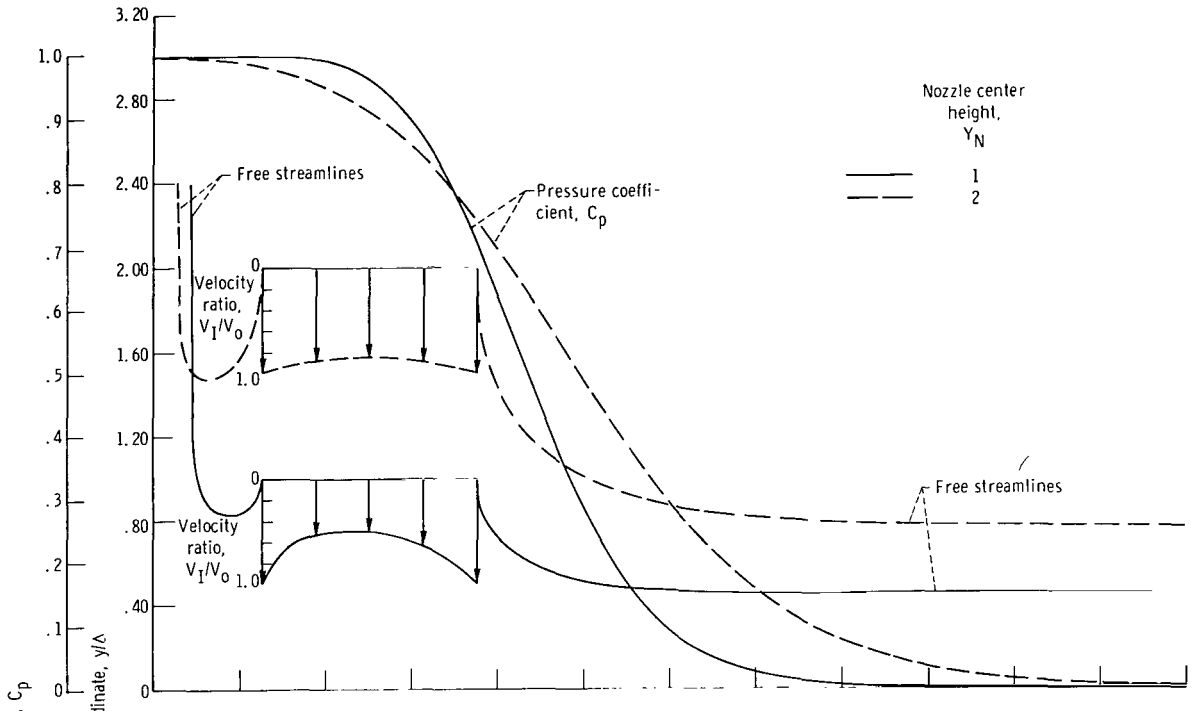

(a) Coordinates of center of nozzle exit plane: $X_N = 1$; $Y_N = 1$ and 2.

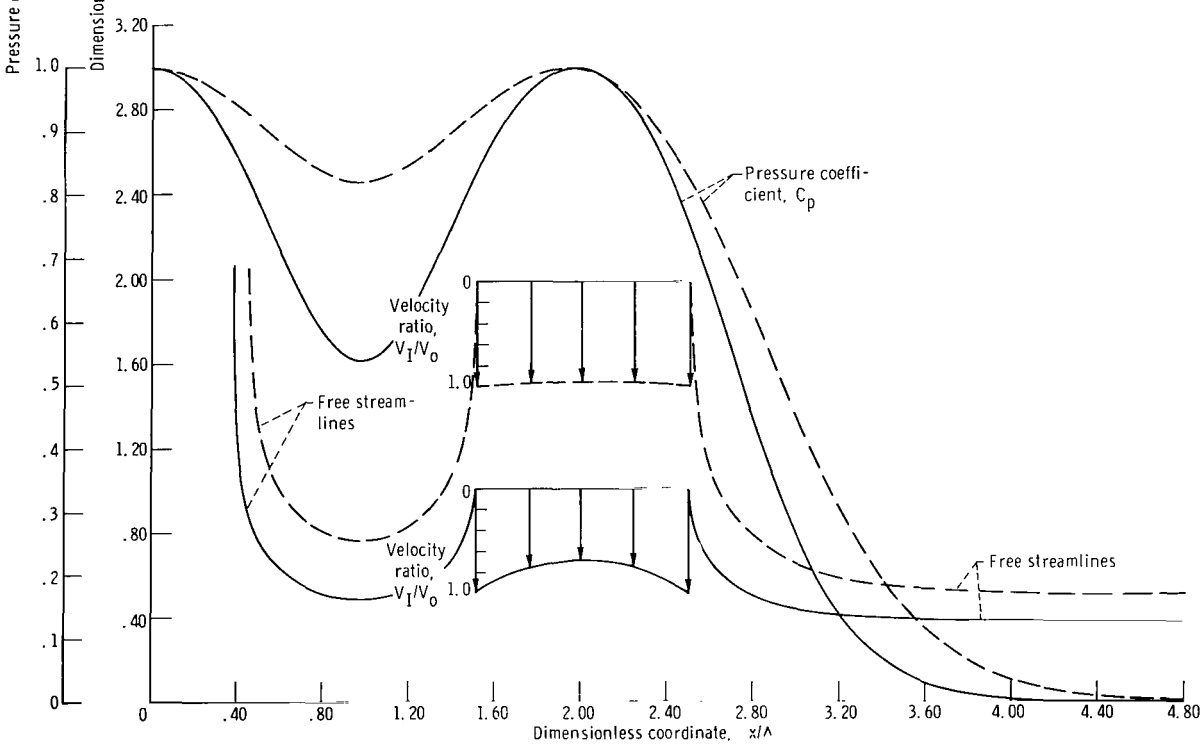

(b) Coordinates of center of nozzle exit plane: $X_N = 2$; $Y_N = 1$ and 2.

Figure 2. - Flow configuration and wall pressure coefficient for 0° nozzle tilt angle.

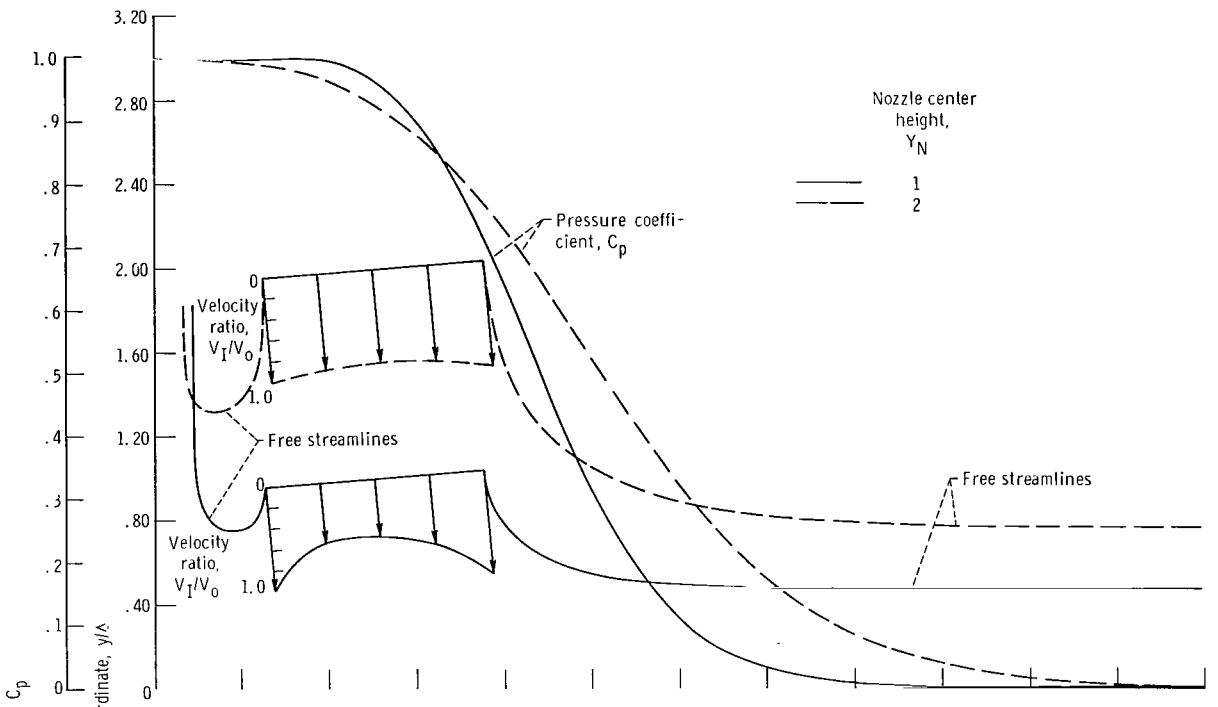

(a) Coordinates of center of nozzle exit plane: $X_N = 1$; $Y_N = 1$ and 2.

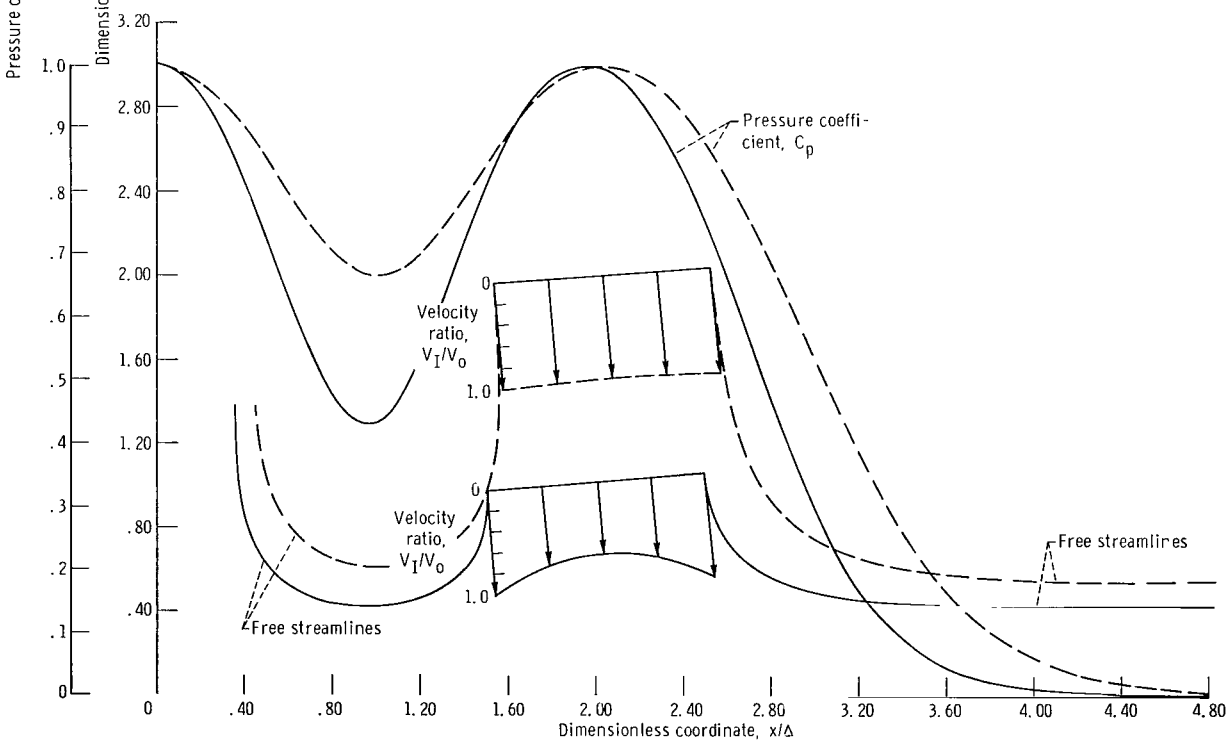

(b) Coordinates of center of nozzle exit plane: $X_N = 2$; $Y_N = 1$ and 2.

Figure 3. - Flow configuration and wall pressure coefficient for 5 nozzle tilt angle.

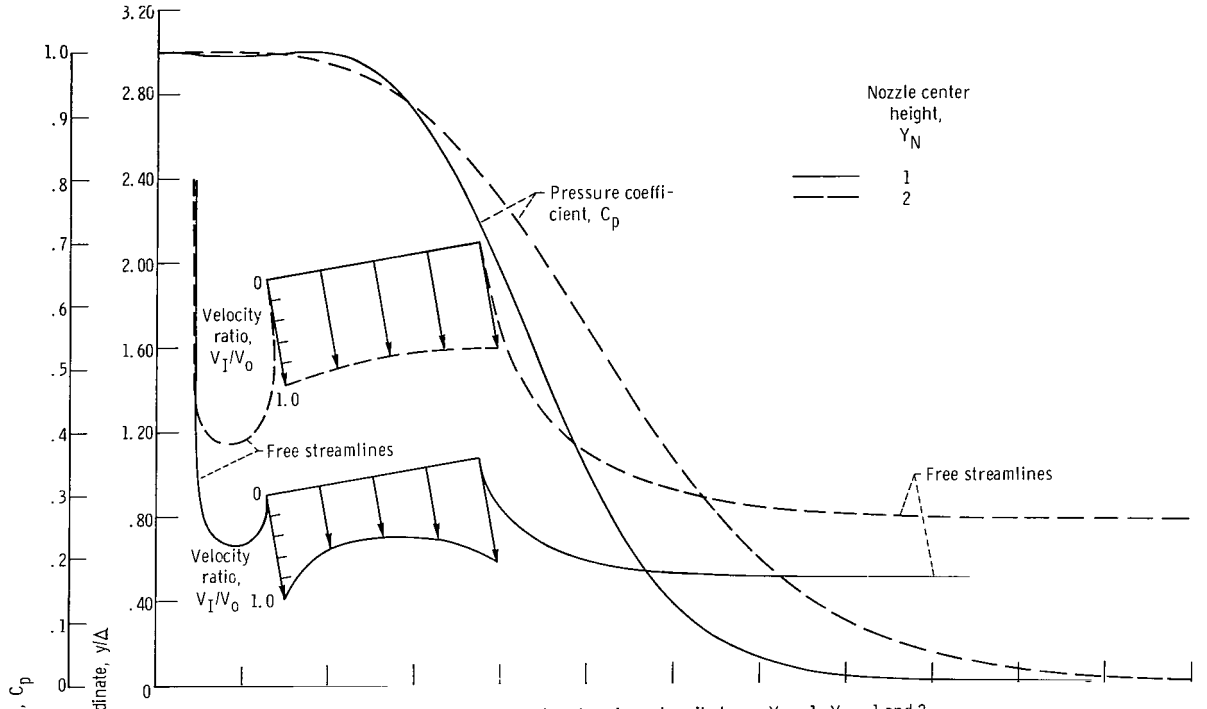

(a) Coordinates of center of nozzle exit plane: $X_N = 1$; $Y_N = 1$ and 2.

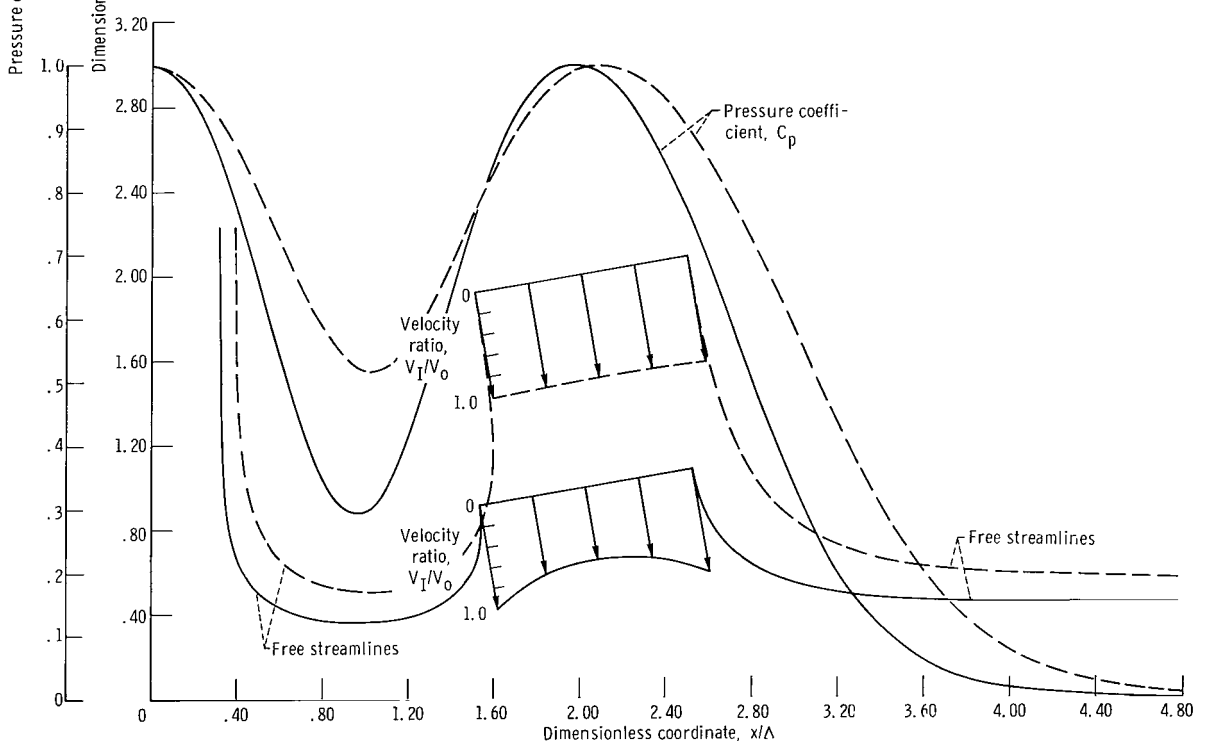

(b) Coordinates of center of nozzle exit plane: $X_N = 2$; $Y_N = 1$ and 2.

Figure 4. - Flow configuration and wall pressure coefficient for 10° nozzle tilt angle.

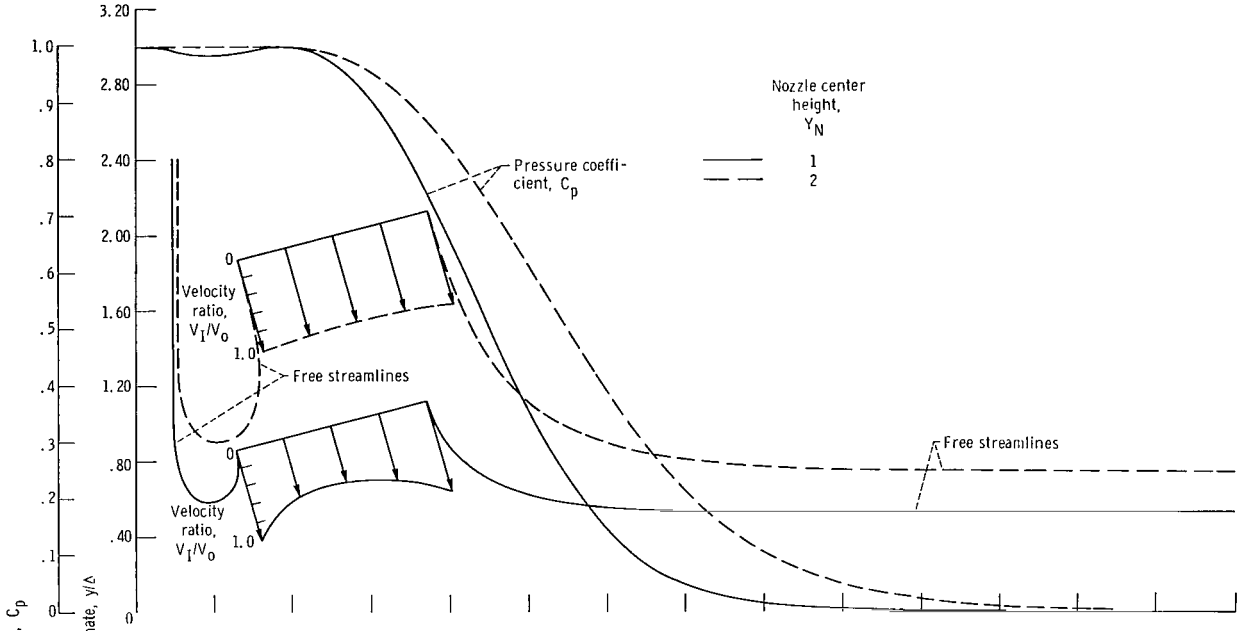

(a) Coordinates of center of nozzle exit plane: $X_N = 1$; $Y_N = 1$ and 2.

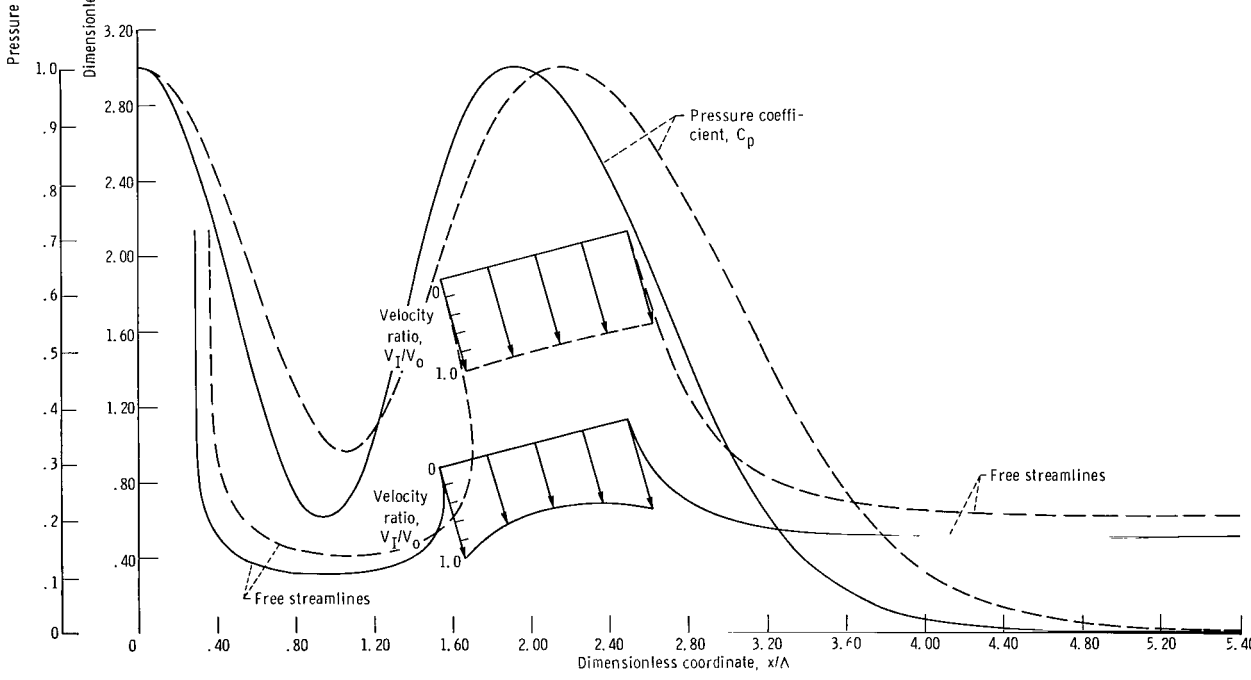

(b) Coordinates of center of nozzle-exit plane: $X_N = 2$; $Y_N = 1$ and 2.

Figure 5. - Flow configuration and wall pressure coefficient for 15° nozzle tilt angle.

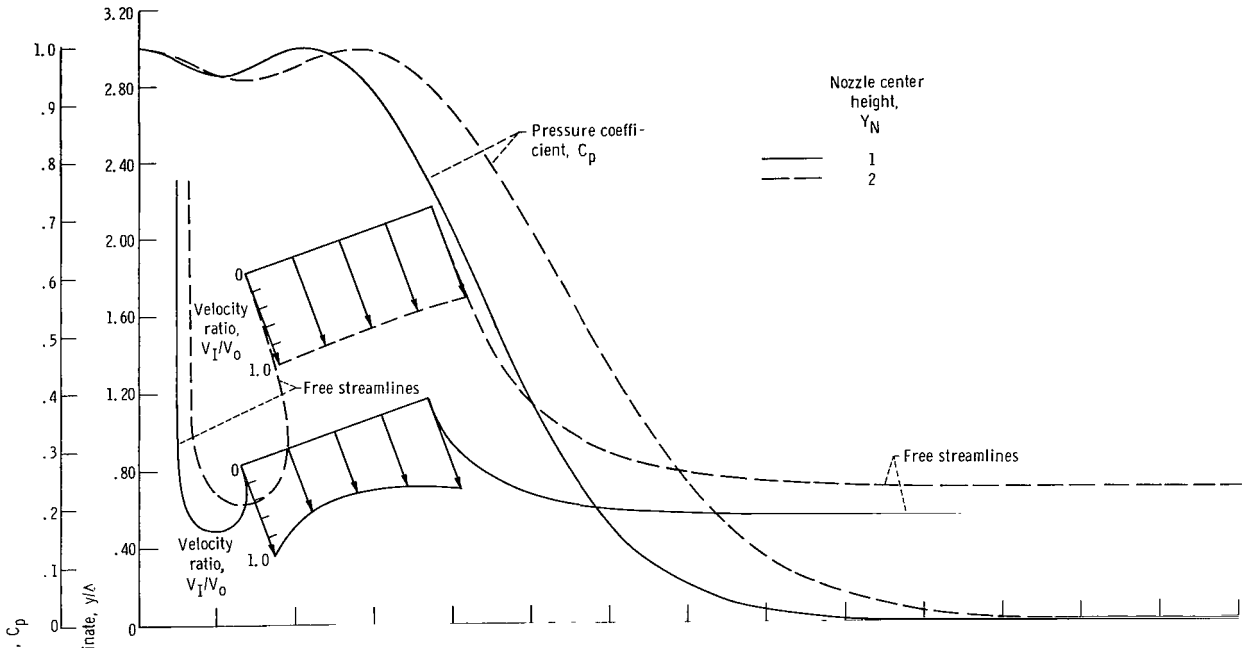

(a) Coordinates of center of nozzle exit plane; $X_N = 1$; $Y_N = 1$ and 2.

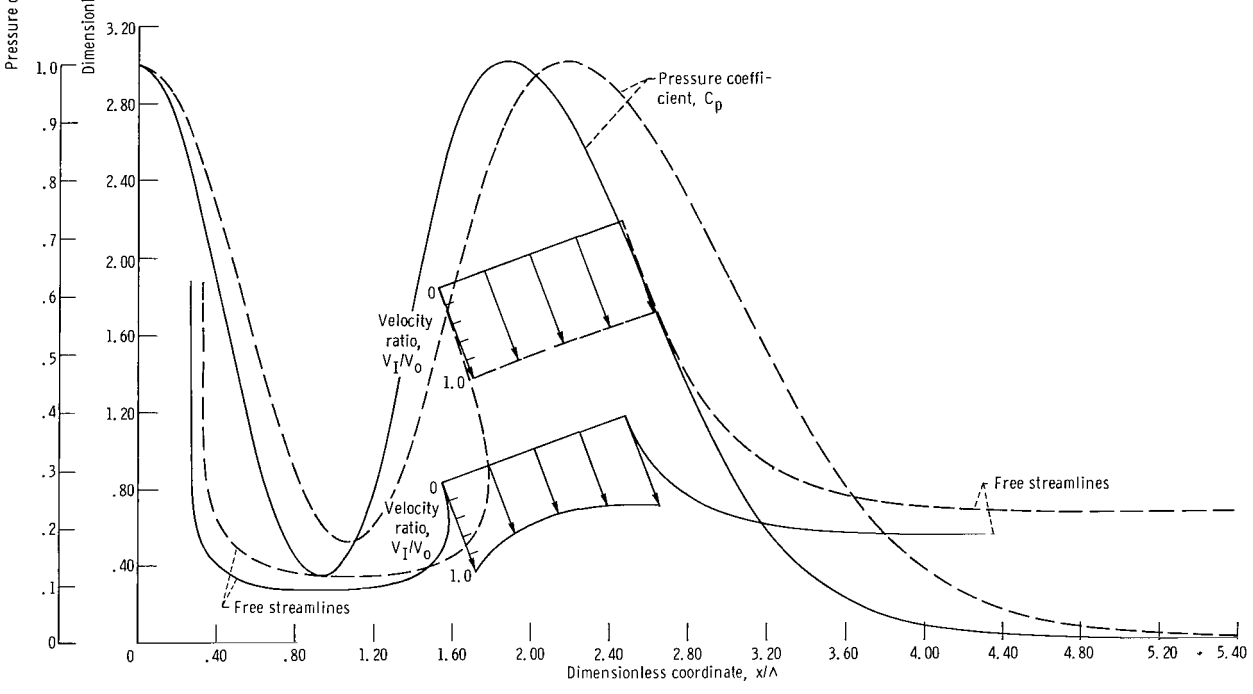

(b) Coordinates of center of nozzle exit plane: $X_N = 2$; $Y_N = 1$ and 2.

Figure 6. - Flow configuration and wall pressure coefficient for 20° nozzle tilt angle.

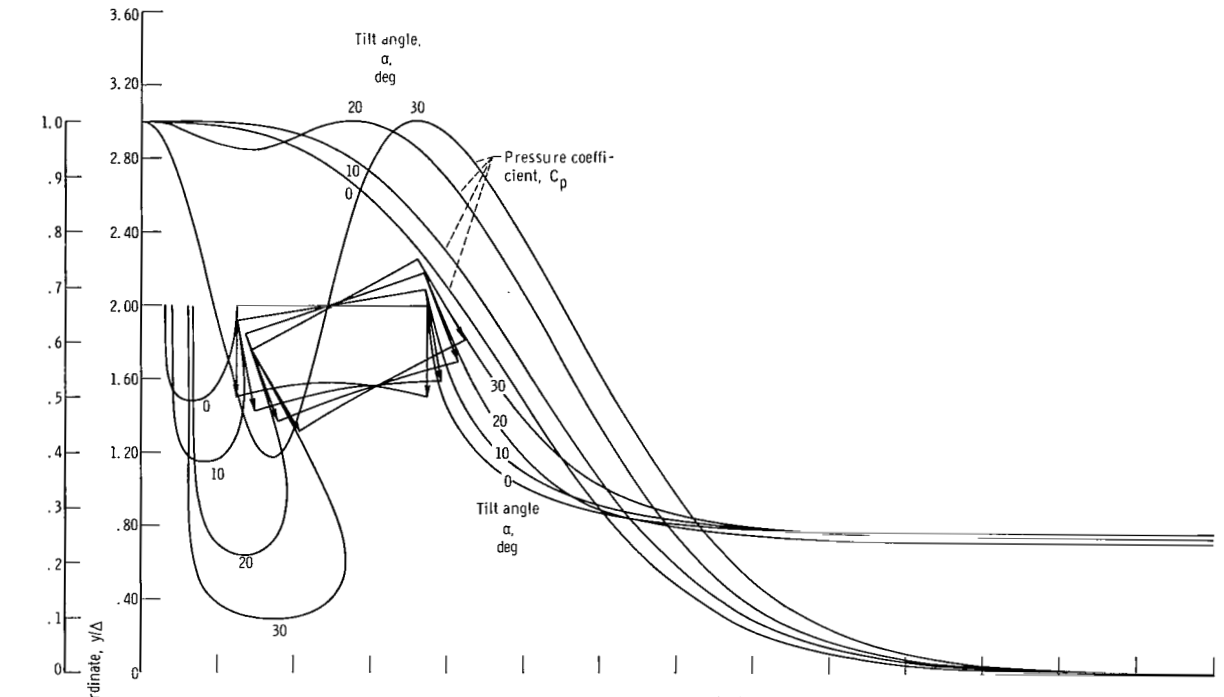

(a) Coordinates of center of nozzle exit plane; $X_N = 1$; $Y_N = 2$.

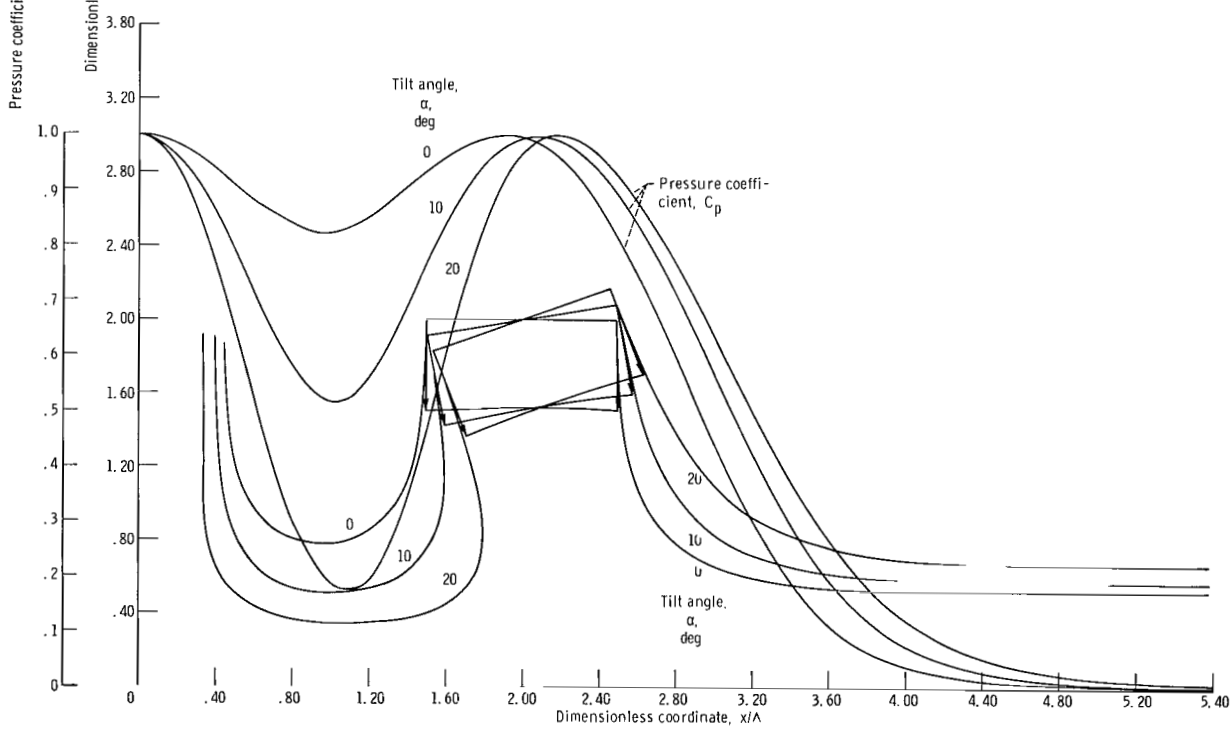

(b) Coordinates of center of nozzle exit plane: $X_N = 2$; $Y_N = 2$.

Figure 7. - Effect of nozzle tilt angle on flow configuration and wall pressure coefficient.

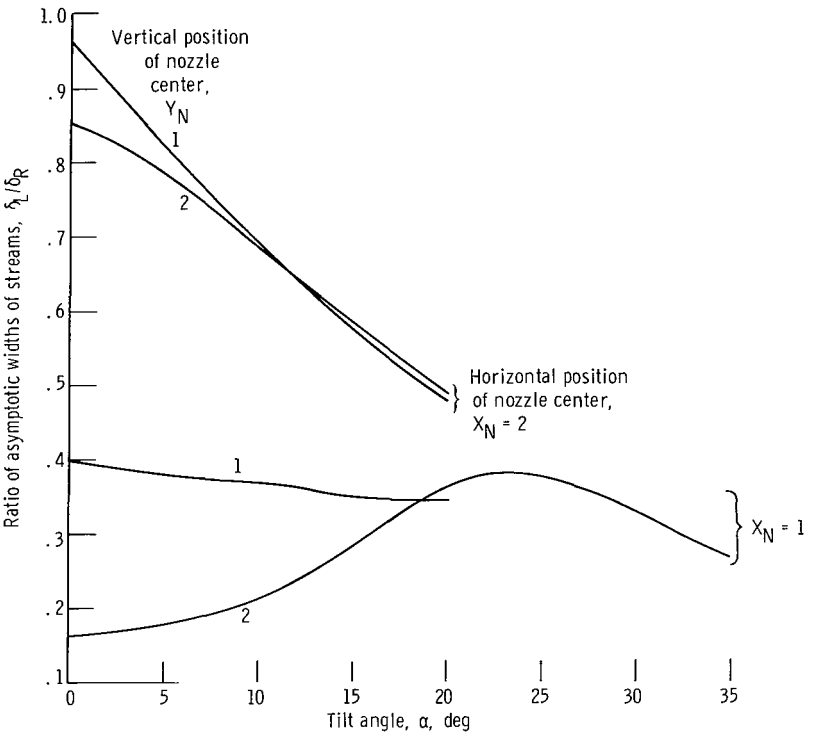

Figure 8. - Variation in ratio of flows with angle for various nozzle positions.

NASA-Langley, 1969 —— 1 E-4639

"The aeronautical and space activities of the United States shall be conducted so as to contribute . . . to the expansion of human knowledge of phenomena in the atmosphere and space. The Administration shall provide for the widest practicable and appropriate dissemination of information concerning its activities and the results thereof."

—NATIONAL AERONAUTICS AND SPACE ACT OF 1958

NASA SCIENTIFIC AND TECHNICAL PUBLICATIONS

TECHNICAL REPORTS: Scientific and technical information considered important, complete, and a lasting contribution to existing knowledge.

TECHNICAL NOTES: Information less broad in scope but nevertheless of importance as a contribution to existing knowledge.

TECHNICAL MEMORANDUMS: Information receiving limited distribution because of preliminary data, security classification, or other reasons.

CONTRACTOR REPORTS: Scientific and technical information generated under a NASA contract or grant and considered an important contribution to existing knowledge.

TECHNICAL TRANSLATIONS: Information published in a foreign language considered to merit NASA distribution in English.

SPECIAL PUBLICATIONS: Information derived from or of value to NASA activities. Publications include conference proceedings, monographs, data compilations, handbooks, sourcebooks, and special bibliographies.

TECHNOLOGY UTILIZATION PUBLICATIONS: Information on technology used by NASA that may be of particular interest in commercial and other non-aerospace applications. Publications include Tech Briefs, Technology Utilization Reports and Notes, and Technology Surveys.

Details on the availability of these publications may be obtained from:

SCIENTIFIC AND TECHNICAL INFORMATION DIVISION

NATIONAL AERONAUTICS AND SPACE ADMINISTRATION

Washington, D.C. 20546